Advantages of Electromagnetic Interferometry Applied to Ground-Penetrating Radar

Non-Destructive Inspection and Characterization of the Subsurface Without Transmitting Anything

Feld, Ralph

DOI
10.4233/uuid:384bf6be-42df-4fba-bba0-0648c7a52e24

Publication date
2017

Document Version
Final published version

Citation (APA)
Feld, R. (2017). *Advantages of Electromagnetic Interferometry Applied to Ground-Penetrating Radar: Non-Destructive Inspection and Characterization of the Subsurface Without Transmitting Anything*. [Dissertation (TU Delft), Delft University of Technology]. https://doi.org/10.4233/uuid:384bf6be-42df-4fba-bba0-0648c7a52e24

Important note
To cite this publication, please use the final published version (if applicable).
Please check the document version above.

The purpose of this PhD-research is to extract useful signal out of electromagnetic noise data, and to develop practical strategies and applications of this technology. We use the technique of creating virtual sources at locations where physical receivers have measured a response, known as seismic interferometry. A receiver measures ambient noise, which carries information about (multiple) reflections in the subsurface. The interferometric methods split what goes into the ground from what comes out of the ground, to extract the response of the subsurface by deconvolution or cross-correlation. The method does not use any information about the actual source's location. Therefore the source can be mobile phone radiation, already available in the air, as long as this background radiation can be represented by uncorrelated noise sources. This is useful for ground-penetrating radar in cases where it is either not allowed to transmit a signal or impossible to place a source, but it is possible to place a receiver.

ISBN 978-94-6295-693-3

Advantages of Electromagnetic Interferometry Applied to GPR

R. Feld

Advantages of Electromagnetic Interferometry Applied to Ground-Penetrating Radar

Non-Destructive Inspection and Characterization of the Subsurface Without Transmitting Anything

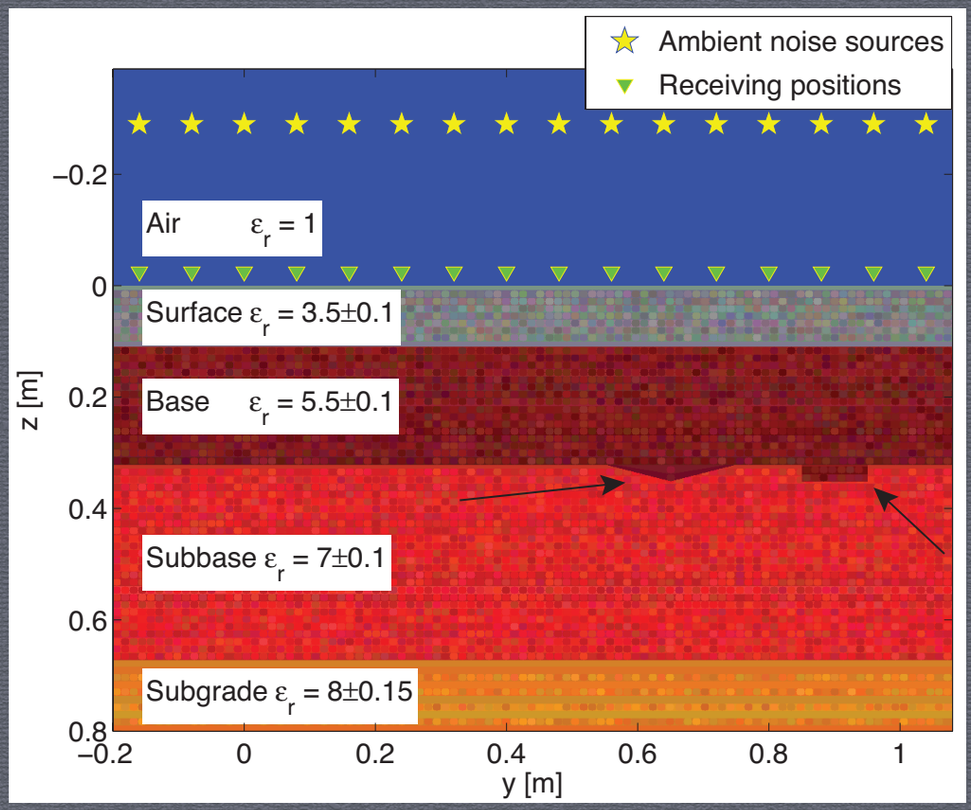

Ralph Feld

Propositions

accompanying the dissertation

Advantages of Electromagnetic Interferometry Applied to Ground-Penetrating Radar

Non-Destructive Inspection and Characterization of the Subsurface Without Transmitting Anything

by

Ralph Feld

1. Electromagnetic interferometry is useful in every frequency band used for visualization purposes, provided that there is uncorrelated background noise in the same band with sufficient signal strength [corollary from this thesis].
2. A more complex model does not necessarily lead to better interferometric results, so that a simpler model has the preference [this thesis, chapter 2].
3. In 10 years each ground-penetrating radar device will have a button 'Passive' for passive cross-correlation measurements [corollary from this thesis, chapter 2].
4. A simpler configuration with lower operational costs suffices for a measurement by analysis by electromagnetic interferometry [corollary from this thesis, chapter 3].
5. It is unethical to improve a tunnel detection tool for border security.
6. A higher education results in a higher salary, but reduces also the chance for a job due to overqualification. Therefore, a higher education is not necessary good for a person. Educated for unemployment.
7. Modern human evolution is not determined by nature, but by cultural taste, the surgical possibilities to adapt to this figure, and the content of the wallet to pay these adaptions.

8. During the doctoral study one learns to distinguish between what is certain and what is uncertain, or, in other words, to question the seemingly logical for the duration that there is no absolute certainty.
9. Someone learns most about one's own culture by studying other cultures.
10. Italian is the worlds easiest language for those who already mastered English.
11. Tailgaters block traffic when they keep driving in front of you.

These propositions are regarded as opposable and defendable, and have been approved as such by the promotor prof. dr. ir. E. C. Slob.

Stellingen

behorende bij het proefschrift

Advantages of Electromagnetic Interferometry Applied to Ground-Penetrating Radar

Non-Destructive Inspection and Characterization of the Subsurface Without Transmitting Anything

door

Ralph Feld

1. Elektromagnetische interferometrie is bruikbaar bij iedere frequentieband die voor visualisatie doeleinden wordt gebruikt, mits er ongecorreleerde achtergrondruis is op diezelfde frequentieband met voldoende signaalsterkte [gevolgtrekking uit dit proefschrift].

2. Een veel complexer model van de ondergrond hoeft niet tot veel betere interferometrische resultaten te leiden, waardoor een simpel model de voorkeur heeft [dit proefschrift, hoofdstuk 2].

3. Over 10 jaar heeft iedere bodemradar een knop 'Passive' voor passieve kruis-correlatie metingen [gevolgtrekking uit dit proefschrift, hoofdstuk 2].

4. Door analyse met elektromagnetische interferometrie voldoet een simpelere meetopstelling met lagere operationele kosten voor een meting [gevolgtrekking uit dit proefschrift, hoofdstuk 3].

5. Het verder ontwikkelen van tunneldetectie gereedschap voor grenscontrole is onethisch.

6. Een hogere opleiding resulteert in een hoger salaris, maar ook in een kleinere kans op een baan door overkwalificatie. Een hogere opleiding is daarom niet per sé goed voor iemand. Opgeleid voor de werkeloosheid.

7. Moderne evolutie van de mens wordt niet bepaald door de natuur, maar door wat cultureel geaccepteerd wordt, de chirurgische mogelijkheden om zich hier op aan te passen en de inhoud van de portemonnee om deze aanpassingen te kunnen bekostigen.

8. Tijdens het promotietraject leer je het zekere van het onzekere te scheiden, oftewel het schijnbaar logische in twijfel te trekken zolang er geen absolute zekerheid over is.

9. Je leert het meest over je eigen cultuur door andere culturen te bestuderen.

10. Italiaans is 's werelds makkelijkste taal voor diegenen die al Engels beheersen.

11. Bumperklevers blokkeren de doorstroom wanneer ze voor je blijven rijden.

Deze stellingen worden opponeerbaar en verdedigbaar geacht en zijn als zodanig goedgekeurd door de promotor prof. dr. ir. E. C. Slob.

Advantages of Electromagnetic Interferometry Applied to Ground-Penetrating Radar

Non-Destructive Inspection and Characterization of the Subsurface Without Transmitting Anything

Advantages of Electromagnetic Interferometry Applied to Ground-Penetrating Radar

Non-Destructive Inspection and Characterization of the Subsurface Without Transmitting Anything

Proefschrift

ter verkrijging van de graad van doctor
aan de Technische Universiteit Delft,
op gezag van de Rector Magnificus prof. ir. K.C.A.M. Luyben,
voorzitter van het College voor Promoties,
in het openbaar te verdedigen op donderdag 7 september 2017 om 10:00 uur

door

Ralph FELD

natuurkundig ingenieur,
Technische Universiteit Delft,
geboren te Poortugaal.

Dit proefschrift is goedgekeurd door de

promotor: prof. dr. ir. E. C. Slob

Samenstelling promotiecommissie:

Rector Magnificus,	voorzitter
Prof. dr. ir. E. C. Slob,	Technische Universiteit Delft
Onafhankelijke leden:	
Prof. dr. ir. C. P. A. Wapenaar	Technische Universiteit Delft
Prof. dr. A. Yarovoy	Technische Universiteit Delft
Prof. dr. ir. J. van der Kruk	Forschungzentrum Jülich GmbH
Dr. ir. B. -J. Kooij	Technische Universiteit Delft
Dr. ir. J. W. Thorbecke	Cray/Technische Universiteit Delft

TU Delft Delft University of Technology

ISES

Netherlands Research Centre for Integrated Solid Earth Science

Keywords: auto-correlation, advanced pavement model, cross-correlation, deconvolution, 2.5D line-configuration, electromagnetic interferometry, ground-penetrating radar, GPR, mono-static GPR, passive interferometry, pavement damage.

Printed by: Proefschriftmaken.nl

Front: Heterogeneous pavement model with two irregular-shaped misalignments between the base and subbase layer (marked by arrows). This Figure illustrates pavement damage inspection by moving a receiving antenna over the surface. The difference with classical non-destructive detection is that nothing is transmitted. It is part of Figure 2.6.

Back: R. Feld

ISBN 978-94-6295-693-3

An electronic version of this dissertation is available at
http://repository.tudelft.nl/.

I dedicate this thesis to my father and mother,
and to both my grandmothers

Ik ben zo trots!

Herina Kodong, August 2016
My 91-year-old grandma at seeing the manuscript of this thesis
18 September 2016 she passed away after a short illness

Contents

Summary

Ground-penetrating radar (GPR) is a non-destructive method that images the subsurface using radar. A transmitter generates a radar pulse. This signal propagates into the ground where it reflects against subsurface heterogeneities, and travels back to the surface. A receiver records the reflected signal. The reflected signal contains information about the subsurface. GPR is useful for pavement- and structures- inspection, object-detection, and characterization of the subsurface. For example, many forms of pavement damage of highways originate in the bottom layers and are invisible until the pavement cracks come to surface. GPR can indicate pavement damage before it is visible at the surface, so that preventive actions can be performed where necessary.

We work towards developing GPR without the need to transmit any signal. Instead, we use signals that are already available in the air, such as mobile phone signals. A technique called electromagnetic interferometry selects those signals that are measured before they enter the ground and after they reflect. It extracts the path from receiver to subsurface and back to the receiver. The result looks as if the receiver has transmitted a signal, while no signal was transmitted by that receiver. This receiver is called a virtual source. By repeating this step for many receiver combinations we create a virtual dataset. This virtual data provides a well-interpretable image of the subsurface.

When we use a single receiver it does not matter whether available actual sources of electromagnetic wave fields are uniformly distributed or are accumulated somewhere. Or whether sources transmit continuously or only every now and then, as long as the measurement records are long enough. The exact measurement time is not important. These effects influence the interferometric result only to a limited extent. This robustness for actual source behaviour makes the concept look realistic.

When we use multiple receivers the resulting data would allow for determining specific material characteristics in the subsurface with respect to a virtual source in a 3D environment. In practice a shortage of receiving antennas or a large distance between subsequent receiving antennas in the line-array can also affect the result. The latter for example due to the physical sizes of the antennas with their housing. Still, the method could work well.

This method is advantageous in cases where signal transmission is impossible, forbidden, or cumbersome, while using a receiver is possible. For example, this is the case when the desired transmission frequency is reserved for mobile communication. The method is specifically advantageous for monitoring applications, because the receiver can stay at a fixed position. The positions of the transmitters are irrelevant, since electromagnetic interferometry provides the result with respect to a signal of the fixed position of the receiver. When using a line-array of

N receivers the method simplifies the setup and reduces the operational costs with respect to traditional GPR, because the analysis provides N^2 virtual data traces out of N actual data traces.

Samenvatting

Bodemradar is een niet-destructieve methode die de ondergrond in beeld brengt door middel van radar. Een transmitter genereert een radarpuls. Dit signaal penetreert de grond en reflecteert tegen de onderliggende structuur. Een ontvanger meet dit gereflecteerde signaal. Het gereflecteerde signaal bevat informatie over de ondergrond. Bodemradar is nuttig voor wegdek- en structuur- inspectie, objectdetectie en kenschetsing van de ondergrond. Veel soorten beschadigingen van geasfalteerde wegen ontstaan in de ondergrondse lagen en blijven onzichtbaar totdat de scheuren aan het oppervlak komen. Bodemradar kan deze schade detecteren voordat ze zichtbaar is aan het oppervlak, zodat preventieve maatregelen kunnen worden genomen.

Wij werken aan de ontwikkeling van een bodemradar die geen zendsignaal nodig heeft. In plaats daarvan gebruiken we signalen die al in de lucht aanwezig zijn, zoals bijvoorbeeld mobiele telefoon-signalen. Een techniek bekend als elektromagnetische interferometrie selecteert signalen die zowel vóór de penetratie in de grond gemeten zijn als na reflectie met de ondergrond. Het isoleert ook het pad van ontvanger naar ondergrond en terug naar de ontvanger. Het resultaat ziet er dan uit alsof de ontvanger een signaal heeft uitgezonden, terwijl in werkelijkheid niets is uitgezonden door die ontvanger. Deze ontvanger heet dan een virtuele bron. Door deze stap te herhalen voor een aantal ontvanger combinaties maken we een virtuele dataset. Deze virtuele data geeft een goed interpreteerbare afbeelding van de ondergrond.

Wanneer we één ontvanger gebruiken maakt het niet uit of de beschikbare werkelijke bronnen van elektromagnetische golfvelden evenredig verdeeld zijn of zich ergens ophopen. Of dat de bronnen constant zenden of slechts zo nu en dan, zolang de meetopnamen lang genoeg zijn. De precieze meettijd doet er dan ook niet toe. Er is slechts een geringe invloed van deze effecten op het interferometrisch resultaat. Deze robuustheid bij het gedrag van werkelijke bronnen maakt het concept realistisch.

Wanneer we meerdere ontvangers gebruiken zouden we specifieke materiaaleigenschappen in de nabije ondergrond kunnen bepalen ten opzichte van een virtuele bron in een 3D wereld. In praktische situaties kan het resultaat ook worden beïnvloed door een te kort aan ontvangende antennes of een te grote afstand tussen opeenvolgende antennes in de lijnopstelling. Dit laatste bijvoorbeeld vanwege de fysieke afmetingen van de antennes met behuizing. Desondanks zou de methode goed kunnen werken.

Deze methode is voordelig in gevallen waarin zendsignalen niet mogelijk of verboden zijn, terwijl er wel een ontvanger gebruikt kan worden. Bijvoorbeeld wanneer de gewenste zendfrequentie gereserveerd is voor mobiele telefonie. Vooral voor controle doeleinden is de methode voordelig, omdat de ontvanger op een

vaste positie kan blijven. De posities van de zenders doen er niet toe, want elektromagnetische interferometrie geeft het resultaat ten opzichte van een signaal van de vaste positie van de ontvanger. Bij N ontvangers in een lijn-opstelling maakt de methode de opstelling simpeler en het verlaagt de operationele kosten aanzienlijk in vergelijking met traditionele bodemradar, omdat de analyse N^2 virtuele datalijsten verschaft uit N werkelijke datalijsten.

Preface

Waiting for the fire to light
Feeling like we could do right
Be the one that makes tonight
'Cause freedom is a lonely road

Calvin Harris and Alesso song, 2013

In this chapter I summarize my personal history leading to this PhD thesis. The main focus is about the PhD, and I describe what I learned at different stages of my academic life. I start by flashing back to my early academic.

The most important skills acquired during my bachelor Applied Physics at Delft University of Technology (TU Delft) where analytical and problem solving skills. After my bachelor thesis fundamental research-project about analysis of the intensity of zero-mode waveguides to study single molecule activity of telomerase, I looked for more applicable work, which I found in industry. I performed an internship at TNO Defence, Security and Safety about temperature measurements of fireworks, to make firework environment-friendly, in collaboration with Philips Lightning. I noticed I also desired to contribute even more to society, which I found at the Reactor Institute Delft (RID). My master thesis was about the development of instrumentation for assessment of radioactivity in excreted urine. The purpose was to measure the amount of radioactive material in the human body after treatment. For this I developed complex instrumentation, tested diverse detectors in cooperation with Canberra Industries, set up experimental research at the RID and at the Erasmus Medical Centre in Rotterdam, and I developed a mathematical-physical model. After one year the research needed to be rounded off to obtain the Master of Science, or engineering degree, in Applied Physics at TU Delft. During my master I learned to apply my analytical and problem solving skills in the real world. At own expenses I continued to build the developed device at the faculty of Industrial Design Engineering during half a year. From this I learned that even one and half year is too short to achieve and finish a bigger project. During a PhD one gets multiple years for a project, and the possibility to share the ongoing research in the field by presenting at conferences, and writing conference and journal articles. The idea to present as expert to other experts from all over the world motivated me to start a PhD in Applied Geophysics at TU Delft.

Despite being at a University of Technology, the project unfortunately initiated very fundamental. I put myself the aim to find practical purposes of the project. It took me about 5 years to finish this research and write this thesis, which is less time than almost *all* colleagues in our hallway needed. I never expected such practical

purposes would follow out of such fundamental theories. I also did not expect how much influence my work would have during conferences.

In 2014 I attended my first conference in Brussels. I was sent alone, and I appeared only one of the few Dutch as well. I had no idea about what to expect, and I did not know anyone. *And I got awarded the best paper poster presentation award, and invited for a 90 euro dinner!* I met a lot of people and felt I belonged in the field of ground-penetrating radar, because I had a mutual understanding with those folks. They thought like physicists, whereas geophysicists aren't able to communicate without their jargon.

Some people became close friends rather than colleagues for the time-being of the conference, and at the end of the week we split up to literally the other ends of the world, often to never see each other again. At some point I discovered that I could take holidays and I used them wisely to travel and to improve my Italian language skill at the International House Milan in Italy. I met many travelers from different cultures. Some were just following their dreams. I was one of those. Some were carrying views that I would never have thought about myself. This extended my experience with different cultures tremendously. An important learning experience was to enjoy the moment fully, or get everything out of the moment, and not think about tomorrow, because then people move on, or feelings change.

In 2015 I attended a conference in Florence and contributed by an oral presentation. My presentation was innovative (GPR without transmitting anything), clear for non-experts, well-researched, and well-prepared. Multiple people told me they were specifically interested in my talk. Of course a part accidentally ended up in my audience, but I got everyone's attention with our innovative ideas and strong scientific evidence. Many questions and discussions followed, making me realize I had become the expert. It was exactly this that made my hard work fulfilling. Some asked my thoughts about their ideas when we met at the next conference in San Francisco, making me realize that Evert and I had built an international reputation. The conference in San Francisco had so many simultaneously ongoing presentations that it was very clear when people ignored other posters to visit mine. That day I inspired many people with my ideas. Those ideas have been extended and made widely available by publishing them as articles in high impact journals to inspire many more people.

And *now* those articles are collected in this book for *you* as reader! I hope the thorough innovation will inspire you! At this moment I would describe my PhD as independent research with the purpose to extract useful signal out of electromagnetic noise data, and to develop practical strategies and applications of this technology. The most important capacity achieved during my PhD is that I learned to recognize information that is trustful, which is together with analytical skills important to lead things in the right direction, to teach myself the right stuff, and to figure things out. The second most important learning experience is that one can always impressively contribute to science, even in a field different than his or her own, although it takes years of research and then you are expert in your topic of the other field.

Ralph Feld

Delft, July 2016

1

Introduction

Tell me why...

Supermode, 2006

Todays world is hard to imagine without radio, TV, and mobile phones. Not everyone knows that these communication techniques are closely related to the inspection method called radar. Radar stands for RAdio Detection And Ranging. It is the technique of imaging by transmitting and receiving electromagnetic signals. When applied to the subsurface it is named ground-penetrating radar (GPR). GPR is useful for non-destructive inspection of infrastructure [1, 2], or characterization of the subsurface. In pavements, many forms of damage originate in the bottom layers and are invisible until the pavement cracks come to surface, where they negatively influence traffic flow and driving safety. GPR is the most important instrument for subsurface health monitoring of infrastructures. GPR can be used to estimate the water content, and other physical properties, because of its sensitivity for changes in electromagnetic material properties. The strengths of GPR are the high resolution to quantify subsurface heterogeneities, and the ability to see both metallic and nonmetallic objects [3].

In 1873 Maxwell predicted the existence of electromagnetic waves, followed by the demonstration of radio waves by Hertz in 1888, and the first wireless signals over a mile distance by Marconi in 1895 [4]. One of the first applications of GPR was glacier mapping in 1929 [5], but most research of the first half of the twentieth century dealt with radio wave propagation above and along the Earths surface for communication and radar [6]. In 1933 transparency of ice and snow to HF radio waves was observed for the 'first' time in Little America [7]. Then, in 1946 aircraft pilots flying over Antarctic ice reported errors in their radar pulsed altimeters [7]. What followed were wave propagation studies in both polar areas for about a decade. In 1960 Greenland tests showed that it can be fatally dangerous to rely on

radar altimetry in poor visibility during low-flights over thick ice [7]. The cause was penetration of radar waves into the subsurface. This led to the use of radar for mapping of ice [8]. Consequently, over the next decade this research extended to other geological materials, for example for coal mining [9, 10] and salt mining [11, 12]. In the beginning of the seventies radar research also focussed on planetary exploration of the moon with Apollo 17 [13, 14]. With technological developments over the years, GPR became in use for a broad spectrum of applications, ranging from hydrological and environmental issues [15], to land-mine detection [16], and forensic investigations [17]. With the evolution of computers 3D visualization became practical [18]. For an extensive historic overview of GPR we refer to Annan (2002) [6], and for an overview of the developed GPR applications over the years we refer to Slob et al. (2010) [3].

The air is filled with radio signals. They can be man-made, such as coming from routers, radio/TV antennas, mobile cell phones, TL-tubes, computerscreens, or naturally occurring, such as cosmic radiation. Communication agencies as the US Federal Communications Commission [19] and the Dutch Agentschap Telecom [20] designate frequencies for specific purposes to avoid interference between the different users. They regulate the spectrum. The maximum power that non-commercial devices like GPR is allowed to transmit gets lower and lower [21]. Hence, both transmission power and frequencies are limited for GPR by laws and regulations.

Traditional GPR considers radio signals other than its own transmitted signal as ambient noise. In this thesis we describe how we propose to use ambient noise for GPR without transmitting any signal. These fields are already in the air and reflect against structures, penetrate, and carry a signature of their path. When the electromagnetic signal is measured before and after its interaction with the subsurface, the common history can be 'divided' out of the data. What remains is a signal like if there would have been a transmitter on our receiving antenna's position, while we actually did not transmit any signal from that antenna position. We call the receiving antenna corresponding to this position a virtual source. GPR without transmitting anything means that we are no longer limited by laws and regulations concerning transmission. Instead, we use these regulations in our advantage, as first proposed by Slob in 2006 [21].

The method of creating virtual sources at physical receivers with known positions is known as (seismic) interferometry. Interferometry by passive sources is also referred to as passive interferometry, to indicate that the sources are uncontrolled. There are good tutorials on (electromagnetic) interferometry available, such as Slob and Wapenaar (2008) [22], and Wapenaar et al. (2010) [23, 24]. Interferometry requires an uncorrelated signal, so the less correlation the better the method works. We assume that the signals in the air are uncorrelated. These signals are continuously changing and therefore interferometry also requires real-time measurements, i.e. ultra-fast sampling in the gigahertz-range. This is still a technological challenge (chapters 2 and 4) [25–27]. However, the technology develops at a rapid pace. At the same time, communication agencies designated the next generations commercial mobile phone frequency bands in or very near a range in which we already can measure in real-time (chapter 2) [27–30].

In this thesis we consider two interferometric methods: interferometry by cross-correlation (CC) and interferometry by deconvolution (IbD). For the case that only one antenna is used, the first method reduces to interferometry by auto-correlation (AC). The second method requires an array of receiving antennas.

1.1. Interferometry by cross-correlation (CC)/auto-correlation (AC) method

In practice, the cross-correlation method provides only phase information. That is great for inspection of the subsurface, because then only phase information is required. It is a simple method. For instance, for the auto-correlation method the virtual source response is proportional to the squared amplitude of the record.

The CC (AC) method delivers amplitude information off by a scale factor, and this result includes information from above the array. Therefore, the other method of interferometry by deconvolution is interesting.

1.2. Interferometry by deconvolution (IbD) method

Both amplitude and phase information are necessary to determine the parameters of the subsurface, to characterize it. The method of interferometry by deconvolution can determine both amplitude and phase information [31]. This method also homogenizes the world above the receiver array. But, an array of receivers is required. In configurations with repetitive measurements over longer timescales that suffer from changing weather conditions the receiving antennas can be placed below the surface out of the reach of these changing conditions. Then reflections from the world above the array is cancelled out with IbD. And it provides data with respect to a virtual source on a chosen receiver's position. This also simplifies the setup and safes operational costs, since there are N^2 virtual sources for N measurements (chapter 3) [32].

IbD is also known under the name interferometry by multi-dimensional deconvolution (MDD) in literature. The part 'multi-dimensional' is only chosen to stress that the world has more than one dimension. There is no convolution in space and therefore no deconvolution in space, unless the world is a 1D world: IbD and MDD are exactly the same, at least in this research.

1.3. The PhD thesis

The aim of this research project is to develop and model practical strategies for electromagnetic interferometry in the frequency band from 10 MHz to 3 GHz, which is the bandwidth of GPR. The purpose is to subtract useful signal out of electromagnetic noise data. One could think about application in areas where the use of controlled sources is not easy.

Each chapter is written independently from the other chapters, so that the reader can step in at the beginning of any chapter. Chapters 2 to 4 start with an abstract of the chapter, an introduction to describe the situation relevant for the chapter, and explains what can be improved. This is typically followed by a detailed expla-

nation of the required theory and numerical model. Then, the numerical results are typically analyzed thoroughly. The chapters continue by describing the application, and finish with a concluding remark.

Chapter 2 discusses non-destructive pavement damage inspection without transmitting anything. In this chapter interferometry by auto-correlation (AC) is investigated and discussed. Chapter 3 describes different antenna line-array configurations for monitoring purposes of GPR. It discusses the exact contribution or trade-off of every step in the interferometry by deconvolution (IbD) and interferometry by cross-correlation (CC) processing for the case of controlled sources. Chapter 4 describes different antenna-array configurations for the case that the sources are uncontrolled. The exact contribution or trade-off of every step in the interferometry by deconvolution (IbD) and interferometry by cross-correlation (CC) processing are discussed. Chapter 5 describes the possible application of passive interferometry for tunnel detection. The research project and this thesis are completed by the main conclusion.

References

[1] C. A. Rodeick, *Roadbed void detection by ground penetrating radar,* Highway and Heavy Construction **127**, 60 (1984).

[2] K. R. Maser, *Detection of progressive deterioration in bridge decks using ground penetrating radar,* in *Experimental assessment of the performance of bridges: Proceedings of the American Society of Civil Engineers/ Engineering Mechanics Division Specialty Conference* (1986) pp. 42–57.

[3] E. C. Slob, M. Sato, and G. Olhoeft, *Surface and borehole ground-penetrating-radar developments,* Geophysics **75**, 75A103 (2010).

[4] S. R. Saunders and A. Aragón-Zavala, *Antennas and propagation for wireless communication systems*, 2nd ed. (John Wiley & Sons, Ltd, 2007).

[5] W. Stern, *Versuch einer elektrodynamischen dickenmessung von gletschereis,* Beiträge zur Geophysik **23**, 292 (1929).

[6] A. P. Annan, *GPR — History, trends, and future developments,* Subsurface Sensing Technologies and Applications **3**, 253 (2002).

[7] A. H. Waite and S. J. Schmidt, *Gross errors in height indication from pulsed radar altimeters operating over thick ice or snow,* Proceedings of the IRE **50**, 1515 (1962).

[8] J. T. Bailey, S. Evans, and G. Robin, *Radio echo sounding of polar ice sheets,* Nature **204**, 420 (1964).

[9] J. C. Cook, *Radar exploration through rock in advance of mining,* Transactions of the Society of Mining Engineers of AIME **254**, 140 (1973).

[10] J. C. Cook, *Borehole exploration in a coal seam,* Geophysics **42**, 1254 (1977).

[11] R. Thierbach, *Electromagnetic reflections in salt deposits,* Journal of Geophysics **40**, 633 (1974).

[12] W. T. Holser, R. J. Brown, F. A. Roberts, O. A. Fredrikkson, and R. R. Unterberger, *Radar logging of a salt dome,* Geophysics **37**, 889 (1972).

[13] A. P. Annan, *Radio interferometry depth sounding: Part I—Theoretical discussion,* Geophysics **38**, 557 (1973).

[14] G. Simmons, D. Strangway, P. Annan, R. G. Baker, L. Bannister, R. Brown, W. Cooper, D. Cubley, J. de Bettencourt, A. W. England, J. Groener, J.-A. Kong, G. La Torraca, J. Meyer, V. Nanda, D. Redman, J. Rossiter, L. Tsang, J. Urner, and R. Watts, *Surface electrical properties experiment,* Apollo 17 preliminary science report (NASA SP-330), Astrogeology Science Center (1973).

[15] R. C. Benson, *Applications of ground-penetrating radar to geotechnical, hydrologic and environmental assessments,* Journal of Applied Geophysics **33**, 177 (1979).

[16] P. Gader, M. Mystkowski, and Y. Zhao, *Landmine detection with ground penetrating radar using hidden Markov models,* IEEE Transactions on Geoscience and Remote Sensing **39**, 1231 (2001).

[17] D. W. Owsley, *Techniques for locating burials, with emphasis on the probe,* Journal of Forensic Sciences **40**, 735 (1995).

[18] M. Grasmueck, *3-D ground-penetrating radar applied to fracture imaging in gneiss,* Geophysics **61**, 1050 (1996).

[19] Federal Communications Commission, www.fcc.gov (2017).

[20] Agentschap Telecom, www.agentschaptelecom.nl/radiocommunications-agency (2017).

[21] E. Slob, D. Draganov, and K. Wapenaar, *Let the FCC rules work for you: Turning commercial noise into useful data,* (GPR2006 conference, Columbus Ohio, USA, 2006).

[22] E. Slob and K. Wapenaar, *Practical representations of electromagnetic interferometry for GPR applications: a tutorial,* Near Surface Geophysics , 391 (2008).

[23] K. Wapenaar, D. Draganov, R. Snieder, X. Campman, and A. Verdel, *Tutorial on seismic interferometry: Part 1 - Basic principles and applications,* Geophysics **75**, 75A195 (2010).

[24] K. Wapenaar, E. Slob, R. Snieder, and A. Curtis, *Tutorial on seismic interferometry: Part 2 - Underlying theory and new advances,* Geophysics **75**, 75A211 (2010).

[25] E. Slob and K. Wapenaar, *Electromagnetic Green's function retrieval by cross-correlation and cross-convolution in media with losses,* Geophysical Research Letters **34** (2007).

[26] R. Feld and E. C. Slob, *Line-array GPR monitoring without transmitting anything,* IEEE Journal of Selected Topics in Applied Earth Observations and Remote Sensing (submitted).

[27] R. Feld, E. C. Slob, and J. W. Thorbecke, *Non-destructive pavement damage inspection by mono-static GPR without transmitting anything,* (submitted).

[28] EU, *Commission proposes to boost mobile internet services with high-quality radio frequencies*, Tech. Rep. (European Commission, Press Release, Brussels, 2016).

[29] T. Wheeler, *Leading towards Next Generation "5G" Mobile Services*, Tech. Rep. (FCC, https://www.fcc.gov/news-events/blog/2015/08/03/leading-towards-next-generation-5g-mobile-services, 2015).

[30] EU, *Radio spectrum: Pascal Lamy presents his report to the Radio spectrum: Pascal Lamy presents his report to the Commission*, Tech. Rep. (European Commission, Press Release, Brussels, 2014).

[31] E. C. Slob, *Interferometry by deconvolution of multicomponent multioffset GPR data,* IEEE Transactions on Geoscience and Remote Sensing **3** (2009).

[32] R. Feld and E. C. Slob, *Validation of interferometry applied to GPR by simulation of possible experimental line-configurations,* IEEE Journal of Selected Topics in Applied Earth Observations and Remote Sensing (submitted).

2

Non-destructive pavement damage inspection by mono-static GPR without transmitting anything

Nobody here knocking at my door
The sound of silence I can't take anymore
Nobody ringing my telephone now
Oh how I miss such a beautiful sound

Armin van Buuren song featuring Trevor Guthrie, 2013

Electromagnetic waves that are already available in the air can be used to create a virtual source. Creating virtual sources at locations where physical receivers have measured a response is known as seismic interferometry. For GPR this can be useful in cases where it is not allowed to transmit a signal, or in cases in which it is not possible to place a source, but is possible to place a receiver. In the case of interferometry by auto-correlation only one receiving antenna is required to retrieve a virtual source response, as if an actual mono-static measurement is performed, without having actually transmitted any signal. The technique can be applied to general 3D heterogeneous media. Examples for a pavement existing of different layers with subsurface damage, modelled with a random heterogeneity only in depth, and modelled with a random heterogeneity in two dimensions. In the first case energy leaks away to the surroundings, but the virtual source response

is still very good. In the second case the result is very similar, so that the simpler 1D heterogeneity seems advantageous in comparison with the 2D heterogeneity. The source distribution, time spreading, and measurement time of the noise sources influence the interferometric result only to a limited extent. The different shapes of pavement damage can be identified for sources distributed uniformly in the sky, as well as for the case of sources only near the horizon. Whether the time spreading of the sources is described by random noise sources that transmit continuous randomly, or by transient noise sources that emit once at a random time, the pavement damage can be identified. The case of transient sources does require much longer records, than with random sources. In general, the method requires relatively long records. The amount of clutter reduces with longer measurement time, but the damage can already be identified in much shorter timescales than what is required for a nice graph with minimal clutter. In this scenario interferometry by auto-correlation seems promising for non-destructive damage inspection without transmitting anything applied to pavements.

Parts of this chapter have been submitted to Geophysical Journal International [1].

2.1. Introduction

The world is covered by pavements, such as highways, bridges, and runways. The quality of these pavements deteriorate during their operational life. Damaged pavement is undesirable for traffic flow and driving comfort and safety. Many forms of damage originate in the bottom layers and are invisible until the pavement cracks come to surface. Ground-penetrating radar (GPR) is a well known technique for non-destructive pavement quality inspection: it is useful for pavement and railroad ballast problems [2, 3], and road evaluation [4–6]. Pavement is smooth and horizontal at the wavelength scale and that makes it relatively easy to calibrate for air-coupled antennas against this surface [7]. Recent developments model typical road damages numerically and show the high potential of GPR in detecting the causes of faults [8, 9]. Here, we extend these models by making them heterogeneous. Then we apply the principles of interferometry to numerically validate GPR measurements without transmitting anything.

Interferometry is a technique that can retrieve a virtual source response at a receiver location. There is already an extensive list of literature in the field of seismic interferometry [10–12] and for electromagnetic interferometry [13–15].

If an electromagnetic wavefield incident from the sky is received before and after its interaction with the ground, interferometry erases the information on the path before the first contact with the receiver. The result is data that would be recorded if there would be a source at the receiver position, see Figure 2.1. The actual source can be controlled (active), i.e. purposefully used in your setup, or uncontrolled (passive), i.e. signals already in the air generated by other sources. Interferometry does not require information about the actual active or passive source positions, orientations, and locations. An actual passive source position might even change during subsequent measurements, while the virtual source location stays fixed at the receiver location. The actual source might be a satellite sending electromagnetic waves to the surface in the bandwidth of radar frequencies, or commercial mobile communication signals, that are already in the air [16, 17]. The use of passive interferometry could therefore be beneficial for monitoring applications or applications where the use of a source is impossible, forbidden, or cumbersome, while using receivers is possible.

In this chapter we investigate GPR by one receiving antenna for non-destructive pavement damage inspection. For this we use the principle of interferometry applied to different 1D and 2D pavement damage models. In the case of 1D heterogeneities there is a limited amount of retrieved events contributing to the final result, creating spurious multiples only when waves are excited at the surface [16, 18]. In the 2D case the amount of retrieved events is much larger. An important difference with the 1D heterogeneous model of Slob & Wapenaar [16] is that we do not use a 1D wave model, i.e. we allow energy to escape to the sides. In this work we use 2D wavefields in 1D and 2D earth models. After this we investigate effects of the source distribution and measurement time, and we compare the results for both random and transient noise sources. We finish by discussing the ability for real measurements.

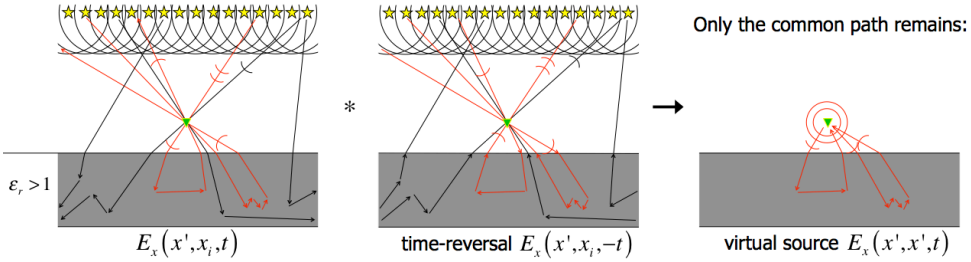

Figure 2.1: Every wavefront, drawn as circles, can be seen as many small sources, denoted by stars, according to the Huygens principle. Here the sources are in far field of the receiver and the earth, and each source has its own random phase. The triangle is the receiver's position. As example some lines are drawn to represent generalized rays. Rays that encounter the receiver before and after they reflect in the medium are colored red. Only these rays will interfere constructively after auto-correlation, or multiplication with its time-reversed record. Other rays, and the parts before the first and after the second encounter with the receiver, will vanish, because only the common path remains after auto-correlation. What is left is a reflection response with respect to a virtual source at the receiver's position. Note that reflection against the surface is not drawn is this scheme, but is taken into account in the models described in this work.

2.2. Interferometry by auto-correlation

Slob & Wapenaar [16] derive the concept of interferometry by auto-correlation. They integrate the Maxwell equations over a volume $\mathbb{D}$ with boundary $\partial\mathbb{D}$, and assume that dissipation is negligible, electric source currents can be described as point sources inside this volume, media are locally smoothly varying near the boundary $\partial\mathbb{D}$, the far-field approximation applies, and that rays that leave the surface perpendicular give the major contribution to the final result. Then they find equation (8) in Slob & Wapenaar [16],

$$\hat{G}^{ee}_{kr}(\boldsymbol{x}_A,\boldsymbol{x}_B)\,\chi_{\mathbb{D}}(\boldsymbol{x}_A)+\left\{\hat{G}^{ee}_{kr}(\boldsymbol{x}_A,\boldsymbol{x}_B)\right\}^{*}\chi_{\mathbb{D}}(\boldsymbol{x}_B) = -\frac{2}{\mu c}\oint_{\boldsymbol{x}\in\partial\mathbb{D}}\left\{\hat{G}^{ee}_{kj}(\boldsymbol{x}_A,\boldsymbol{x})\right\}^{*}\hat{G}^{ee}_{rj}(\boldsymbol{x}_B,\boldsymbol{x})\,d^2\boldsymbol{x}+\text{'ghost'}. \tag{2.1}$$

The hat stands for frequency domain, and $*$ denotes for the complex conjugate. The Greens functions are symbolized as $\hat{G}^{ee}_{kr}(\boldsymbol{x}',\boldsymbol{x})$, with two indices in superscript and two in subscript. The first index denotes the field and the second the source type. The superscripts remind us that the received signal is an electric field generated by an electric current, shown by e. The first subscript represents the direction of the field component, and the second subscript denotes the component of the source current vector. The receiver's and source's positions are represented by respectively the first and second arguments. $\boldsymbol{x}_A$ and $\boldsymbol{x}_B$ are two receiver positions. The characteristic function $\chi_{\mathbb{D}}(\boldsymbol{x})$ of the domain $\mathbb{D}$ is $\chi_{\mathbb{D}}(\boldsymbol{x}) = \{0,1/2,1\}$ for $\boldsymbol{x}\in\mathbb{D}',\partial\mathbb{D},\mathbb{D}$. μ and c stand for respectively the magnetic permeability and the velocity in the medium of the actual sources.

In this paper there is only one receiver at position $\boldsymbol{x}'$ inside volume $\mathbb{D}$, so that

equation (2.1) reduces to:

$$\Re\left\{\hat{G}^{ee}_{kr}\left(\boldsymbol{x}',\boldsymbol{x}'\right)\right\} = -\frac{1}{\mu c}\oint_{\boldsymbol{x}\in\partial\mathbb{D}}\left\{\hat{G}^{ee}_{kj}\left(\boldsymbol{x}',\boldsymbol{x}\right)\right\}^{*}\hat{G}^{ee}_{rj}\left(\boldsymbol{x}',\boldsymbol{x}\right)d^{2}\boldsymbol{x} + \text{'ghost'}. \tag{2.2}$$

$\Re$ denotes the real part of the term within brackets. The right-hand side of equation (2.2) integrates over a boundary $\partial\mathbb{D}$ of actual sources. This equation requires sources surrounding the virtual source position. In reality we do not have this source distribution. A limited source distribution creates 'ghost' events in the interferometric result. In the next paragraph we discuss these non-physical events in more detail. The real part on the left-hand side of the equality sign means that the function is not causal in time-domain, but time-symmetric. The freedom during the whole derivation is the ability to use heterogeneous and anisotropic media.

We define the electric wavefield as

$$\hat{E}_{k}\left(\boldsymbol{x},\omega\right) = \int_{\boldsymbol{x}''}\hat{G}_{kp}\left(\boldsymbol{x},\boldsymbol{x}'',\omega\right)\hat{N}_{p}\left(\boldsymbol{x}'',\omega\right)d^{2}\boldsymbol{x}'', \tag{2.3}$$

$$\hat{E}_{r}\left(\boldsymbol{x},\omega\right) = \int_{\boldsymbol{x}'}\hat{G}_{rq}\left(\boldsymbol{x},\boldsymbol{x}',\omega\right)\hat{N}_{q}\left(\boldsymbol{x}',\omega\right)d^{2}\boldsymbol{x}', \tag{2.4}$$

with random noise sources $\hat{N}_p$ that are band-limited by a Ricker wavelet $\hat{S}(\omega)$. The noise sources are uncorrelated, which means that [13] (with spatial average $\langle\ldots\rangle$):

$$\left\langle\hat{N}_{p}\left(\boldsymbol{x}'',\omega\right)\left\{\hat{N}_{q}\left(\boldsymbol{x}',\omega\right)\right\}^{*}\right\rangle = \frac{1}{\mu c}\delta_{pq}\delta\left(\boldsymbol{x}''-\boldsymbol{x}'\right)\left|\hat{S}(\omega)\right|^{2}. \tag{2.5}$$

Consequently,

$$\left\langle\hat{E}_{k}\left(\boldsymbol{x},\omega\right)\left[\hat{E}_{r}\left(\boldsymbol{x},\omega\right)\right]^{*}\right\rangle = -\operatorname{Re}\left\{\hat{G}_{kr}\left(\boldsymbol{x},\boldsymbol{x},\omega\right)\right\}\left|\hat{S}(\omega)\right|^{2} + \text{'ghost'}. \tag{2.6}$$

We consider a single, horizontal antenna at position $\boldsymbol{x}'$, so that $k = r = 1$. For the sake of the explanation, we write equation (2.6) as

$$\operatorname{Re}\left\{\hat{E}_{1,\text{ virtual}}\left(\boldsymbol{x}',\boldsymbol{x}',\omega\right)\right\} \sim -\frac{1}{\hat{S}}\left|\hat{E}_{1,\text{ measured}}\left(\boldsymbol{x}',\omega\right)\right|^{2}, \tag{2.7}$$

with $\hat{E}_{1,\text{ measured}}\left(x',\omega\right)$ the actual record. This means that the virtual source response is proportional with the squared amplitude of the record, scaled by a Ricker wavelet.

2.3. 1D heterogeneity in a 2D damaged pavement model

The pavement model shown in Figure 2.2 contains three irregular-shaped misalignments between the base and subbase layers (interface C) of 3 cm thickness.

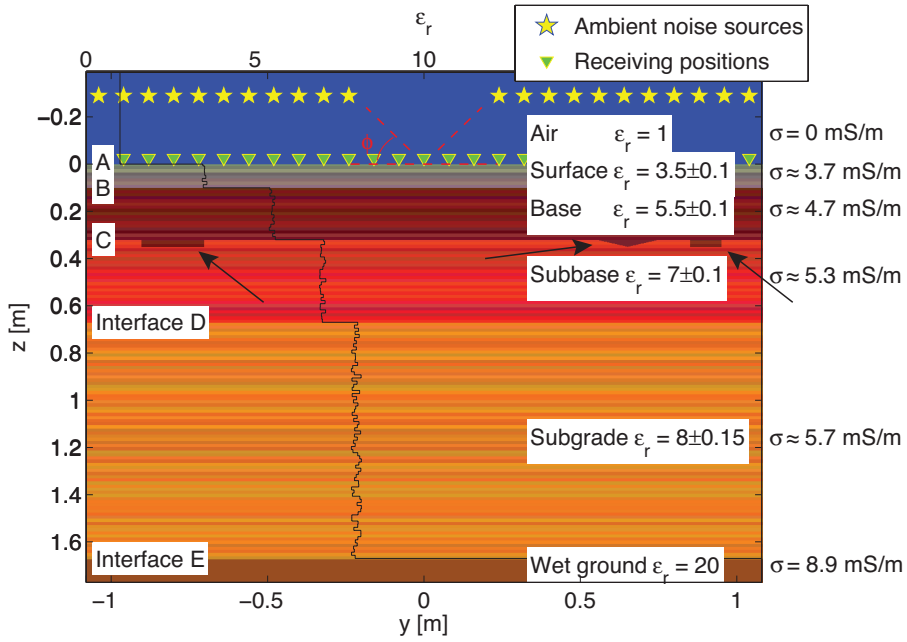

Figure 2.2: 1D heterogeneous pavement model with three irregular-shaped misalignments between the base and subbase layer (marked by arrows). The relative permittivity is plotted w.r.t. the upper axis. B-scan positions are shown schematically.

This example is inspired by a pavement damage model used in Tosti et al. [8]. We apply a random uniform variation in the relative permittivity ε_r within each layer, to introduce irregularities at subresolution scales in the pore volumes and geometries that lead to macroscopic random variations in the permittivity. In the 1D model spatial variations consist of little sublayers with a thickness equal to half of the smallest wavelength in the modeled experiment: 1.32 cm. We use the relative permittivity values ε_r plotted and mentioned in Figure 2.2. The electric conductivity is taken as $2\sqrt{\varepsilon_r} \cdot 10^{-3}$ S/m in the pavement. Note that in literature much lower values for the electric conductivity of pavement can be found. We chose a higher value, because we believe it is more realistic to do so.

A receiving antenna is represented by a lossless, non-reflecting point receiver 2.5 cm above the pavement. Figure 2.2 shows its positions for a B-scan schematically, which means that along the 2 m transect subsequent measurements are made every 2.5 cm. To represent the receiving antenna as point receiver is sufficient for a numerical study to validate interferometry applied to GPR. The only difference with a physical receiver would be a filter-effect, but that would not influence the numerical

validation of the theory. In far-field above the antenna we distribute 250 sources over a 10 m horizontal line (4 cm spacing). The parameters are implemented using the 2D finite difference time-domain code GprMax2D [19]. GprMax2D considers media with frequency independent and isotropic properties. The resulting numerical data is analyzed using a commercial software package [20].

Commercial noise, like for instance mobile communication signals, exists of bandwidths that are so narrow, e.g., mobile phones have about 2x65 MHz bandwidth in the 800 and 900 MHz bands in Europe [21], that it results in wide wavelets with ringing in the time-domain. For explanation purposes we model noise with a wider Ricker-shaped bandwidth, a center frequency of 900 MHz and a random phase. In this numerical experiment we use a long recording time of 697.2 μs to minimize noise in the results after interferometric analysis, so that the effects of the different Earth models studied in this work can be discussed. Then, we auto-correlate the data. Figure 2.3a shows the first 69.7 ns of the data measured at the middle receiver of Figure 2.2. Only the parts that interfere constructively remain.

Based on 1D mean permittivity values we globally estimated the arrival times of primary and multiple reflected waves, for the case that there would have been a virtual source at the receiver's position. The estimated arrival times are marked with solid lines in Figure 2.3. We defined the interfaces in 2.2 and label the subsequent reflecting interfaces in Figure 2.3. For instance, BAB stands for the arrival time for a wave propagating from the receiver (virtual source), reflecting subsequently to interfaces B, A and B, after which it returns to the receiver.

Now, direct reflection correlated with multiple reflection will result in events as well, known as spurious multiples. They arrive before the main direct reflection. Their arrival times have been estimated and marked with a dashed line in Figure 2.3.

Points that do not vanish during the 'integration' of the sources (equation (2.2), and Figure 2.3) are called stationary points. Stationary points create the physical expected events and the spurious multiples. There are also extra events due to the limited source span-width: the integration boundary $\partial\mathbb{D}$ ends at the endings of our 10 m source span-width, and that causes non-physical events. The arrival times of these events are estimated from a similar numerical experiment with controlled sources and marked with a dashed line without label in Figure 2.3. The other events are harder to predict, because they appear with the damage in the pavement, which cause additional stationary points due to their asymmetry.

The Ricker wavelet was used as the band-limitation of our noise and therefore present as $\hat{S}(\omega)\,\hat{S}(\omega)^*$ in the interferometry results, with $\hat{S}(\omega)$ the Ricker wavelet. We divide this wavelet out of the summed traces to be able to compare the results with a reference, see equation (2.7). The comparison is made in Figure 2.3. The events are analyzed as described above. Note how well the reflections of interfaces C and D are retrieved, but spurious events are also clearly visible. Up till now the analysis has been described for one measurement with a receiver. For the B-scan we execute the auto-correlation (AC) analysis for each receiver position, resulting in Figure 2.4. The damage can be identified well (see the vertical arrows). Note, in comparison with the modeled result, the non-physical events just before interfaces

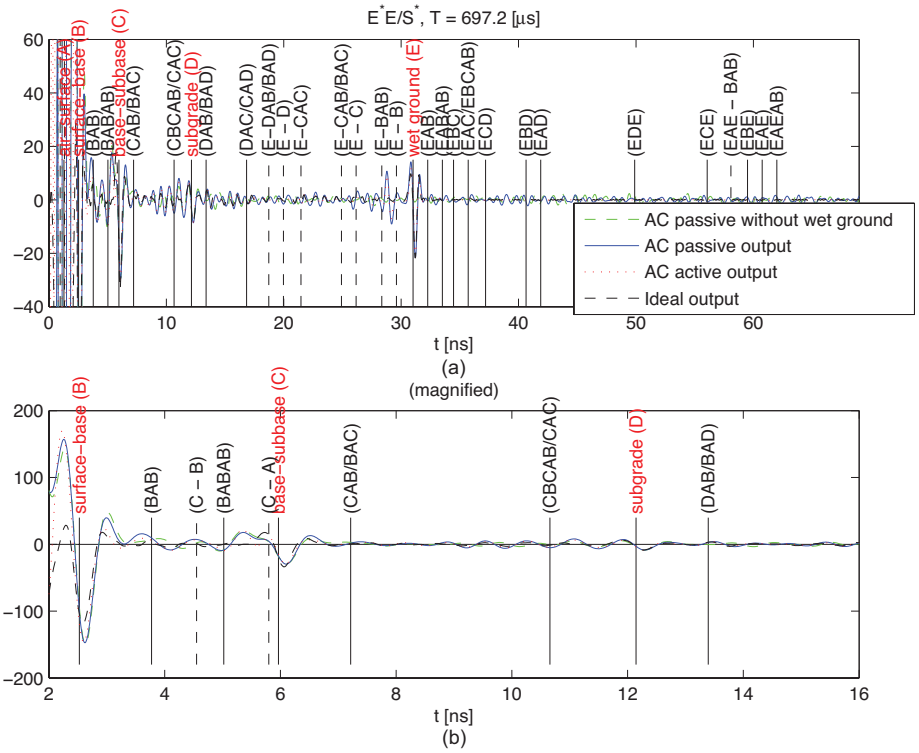

Figure 2.3: (a) Comparison of the auto-correlation result (blue solid) with the modeled result (black dashed) for the middle receiver near the origin in Figure 2.2. The red dotted line provides the active interferometry result, which is the theoretical most optimal result that would be possible for passive interferometry. Also the results for the situation without wet ground is plotted by a green dashed line. (b) The interval 2-16 ns.

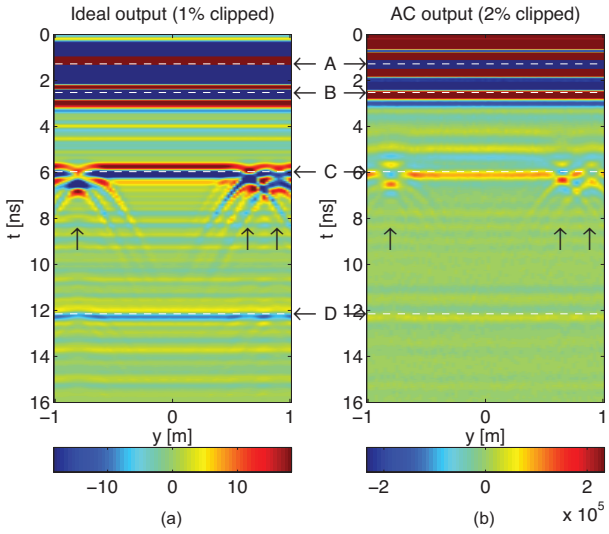

Figure 2.4: Mono-static B-scan over 1D heterogeneous damaged pavement. The interfaces of Figure 2.2 are indicated by dashed white lines and black arrows. The auto-correlation output (b) is compared with the ideal output (a). A part is clipped by limiting the amplitude to the percentile corresponding to the mentioned percentage. Since the maximum amplitude of the AC and ideal outputs differ, different amounts have been clipped. Within the plots the three damages are indicated by arrows.

C, D, and E (marked in Figure 2.4). In Figure 2.5 we look at the difference with respect to the trace in the middle. The result of the autocorrelation data shows that the damage zones can be identified. This suggests that subsurface pavement damage could be identified with passive interferometry.

The wet ground at 1.67 m depth is a strong reflector and almost functions as a mirror, i.e. it mirrors the sources. In this way it approximates the requirement of equation (2.2) to surround the virtual source position by sources. The media are not surrounded by sources on the sides, and energy can leak away. Additional heterogeneities help to scatter the wavefield, so that information from all directions can be received. By introducing 1D heterogeneity the strong reflector at the bottom would not be necessary anymore [16], but, in Figure 2.3 many amplitudes do not overlap completely. Figure 2.3 also contains the result for the geometry without strong reflector E, which is a different but acceptable outcome in comparison to the ideal result. This seems to confirm that the strong reflector is no necessity, which extends the range of possible applications. However, there is no perfect overlap. Apparently, some energy still leaks away through the sides. We research this by introducing a 2D heterogeneity.

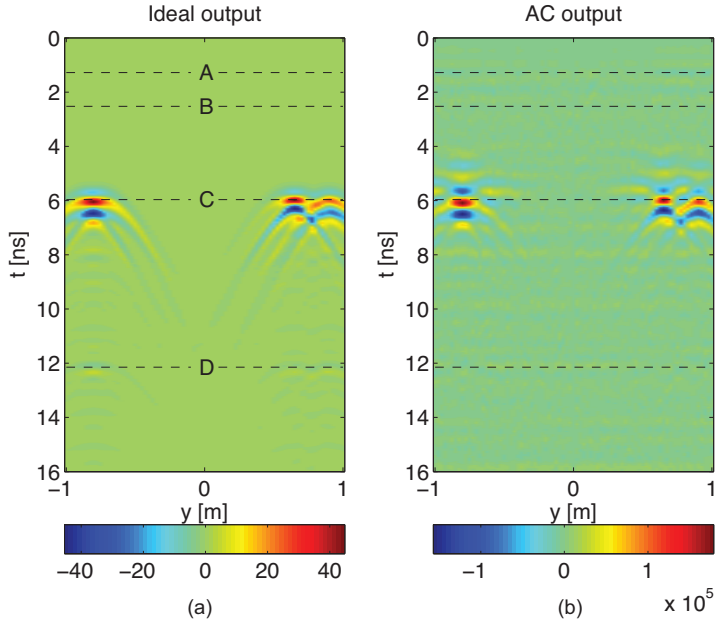

Figure 2.5: As Figure 2.4, but now the difference w.r.t. the trace found in the middle is shown.

2.4. 2D heterogeneity in a 2D damaged pavement model

The 2D heterogeneous zone is 3.4 m wide. The other 6.6 m still consist of many plane layers. The 2D heterogeneity section in the model exists of many layers, with each layer filled up with cylindrically shaped objects with varying relative permittivity and a diameter of 1.32 cm, which corresponds to half the smallest wavelength in the pavement. The thick subgrade exists of small layers with alternating 1D and 2D heterogeneities. Figure 2.6 shows a part of the 2D heterogeneity and the positions for a B-scan schematically.

A 697.2 µs single record from the middle receiver position in Figure 2.6 is auto-correlated. The Ricker wavelet is divided out of the remaining trace, and the result is shown in Figure 2.7. In comparison to the 1D heterogeneous result in Figure 2.3, here the 2D heterogeneous result looks a bit smoother near 10 ns. The correspondence between both lines for the reflection against interface D is less perfect than during the 1D heterogeneous analysis.

Now, 697.2 µs records are made during a B-scan at the positions indicated in Figure 2.6. Each single record is auto-correlated, after which the Ricker wavelet is divided out of the data. Then, the difference with respect to the result at the receiver's position in the middle (Figure 2.6) is considered and shown in Figure 2.8. This result is very similar to the many-layered 1D heterogeneous case of Figure 2.5. The 1D heterogeneous model seems to work slightly better in the subsurface,

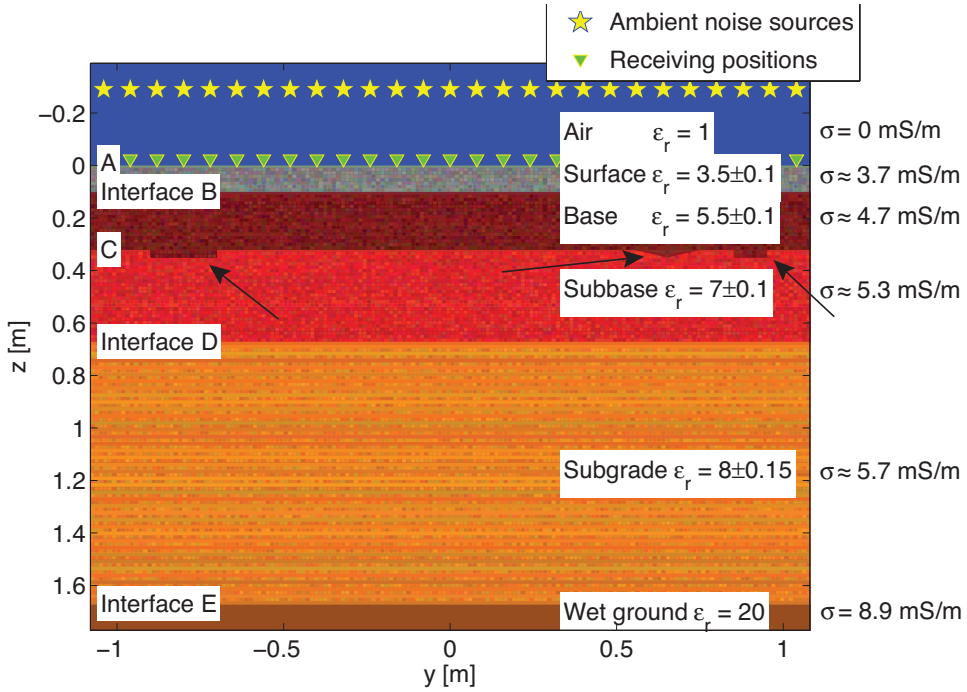

Figure 2.6: 2D heterogeneous pavement model with three irregular-shaped misalignments between the base and subbase layer (marked by arrows). B-scan positions are shown schematically.

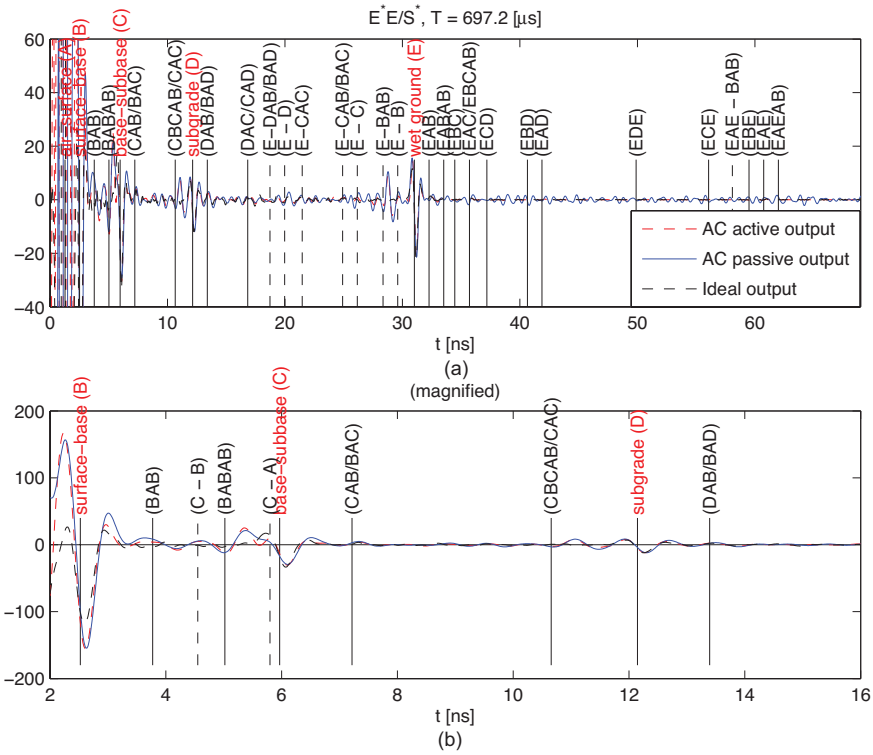

Figure 2.7: (a) Comparison of the auto-correlation output (blue solid) with the ideal output (black dashed) for the middle receiver near the origin in Figure 2.6. Also the active interferometric output is drawn. (b) The interval 2-16 ns.

while the 2D heterogeneous model seems to work slightly better in the subbase and subgrade. This suggests that there is no significant advantage of using the 2D heterogeneity in comparison to the 1D heterogeneity. Therefore, the simpler 1D heterogeneity is recommended for use. Especially if one wants to extend the model to 3D.

2.5. Effect of the source distribution

Apart from the heterogeneity of the medium, also the source distribution can affect the interferometric procedure. According to Huygens principle every wavefront can be seen as many small sources. For this reason the wavefront is represented by sources distributed over a line. However, in this section we consider the effect of the angle of the incoming wave, or the effect of a source distribution on the sides. Figure 2.2 defines the angle ϕ between the surface and the highest source. For simplicity we assume symmetry in the spatial positions of the sources. ϕ can depend on the distance between humans with mobile phones and the receiver, or

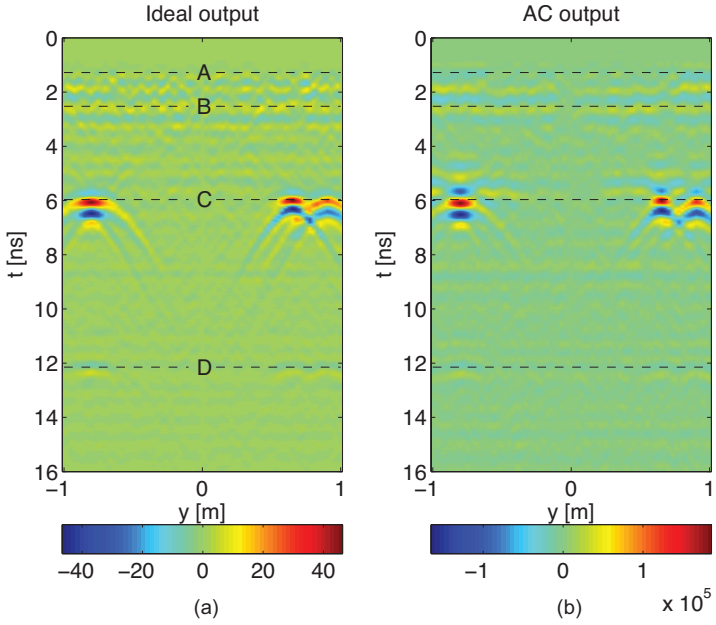

Figure 2.8: Mono-static B-scan over 2D heterogeneous damaged pavement (Figure 2.6) by auto-correlation. The difference w.r.t. the trace found in the middle is shown.

by apartment or office buildings in height. By interferometry by auto-correlation the B-scan result is retrieved for different angles ϕ, see Figure 2.9. Although the result is best with a full source distribution, an angle of 5 degrees with respect to the horizon is still sufficient to identify the different shapes of pavement damage. One might discuss whether it is worth investigating an asymmetric source distribution. In some specific cases an asymmetric source distribution might be found during measurements at the border between habited and inhabited areas. Instead, for practical purposes the effect of the measure time is discussed in the next section.

2.6. Effect of the measure time

During a real experiment in the field a not unimportant aspect is the measure time T. Ideally one gets a sufficient quality data in a reasonable amount of measure time. The method of interferometry by auto-correlation requires relatively long records. Figure 2.10 shows the interferometric results for different record timelengths T varying from 17 µs up to almost 700 µs. The amount n of sources per unit time has been kept constant during these simulations. Pavement damage can be identified with all record time lengths. However, longer measure times provide less clutter in the results.

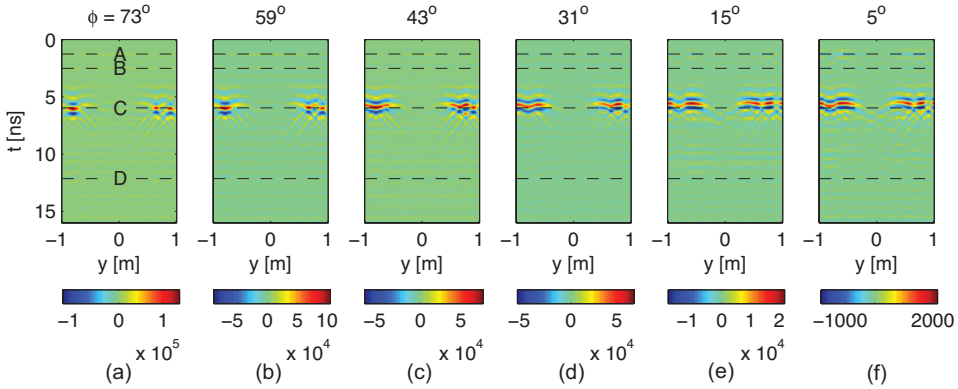

Figure 2.9: Analysis of the influence of the incident angle ϕ.

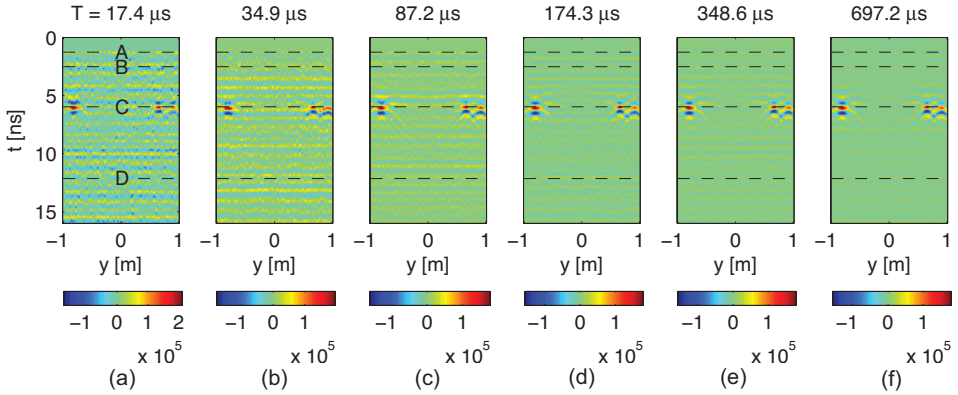

Figure 2.10: Analysis of the influence of the measure time.

2.7. Effect of sparser noise sources

Till now the noise was modelled as a Ricker-shaped bandwidth, a center frequency of 900 MHz and a random phase. An alternative of this random noise are transient noise sources. Transient noise sources are sources that emit once at a random time, resulting in a sparse spectrum, while random noise sources can transmit continues randomly. Figure 2.11a shows an example of the spectrum of transient noise sources, and Figure 2.11b the spectrum of random noise sources. The effect of the amount n of transmitting sources per unit time on the interferometric result is investigated and shown in Figures 2.11c-g. Note that tranient noise causes additional clutter in the graphs. Even with 29 transmitting sources per ms in 697.2 µs records pavement damage can be identified. The effect of the measure time for a constant amount n of transmitting sources per unit time of 465 sources per ms is displayed in Figures 2.11h-l. Note that longer time records are considered, from 174 µs to 2.789 ms, than in Figure 2.10. With 465 sources per ms and 174 µs time records the pavement damage can still be identified. This suggests that the method also applies in areas where commercial noise is sparser distributed.

2.8. Discussion: real commercial noise

In the end, real commercial noise should be used, like for example mobile phone signals. In most cases the electromagnetic field strength is around 1 V/m on the street, although strengths of 5 mV/m have been reported, and even 1 mV/m, although the latter one was measured in the 1800 MHz band [22]. Taking note of the ratio between the amplitudes of the direct wave and the reflection corresponding to interface C, we estimate the field strength of the reflection to be more or less 3.8 mV/m, which seems sufficient to be measured.

However, we have no control over the sources, so that subsampling cannot be used. Therefore the commercial noise should be measured in real-time, which will not be an easy task. At the moment, commercially available GPR systems cannot perform real-time measurements [16, 23] in the 800 and 900 MHz bands. In Chapter 4 we extend this discussion about the available GPR systems. However, around the year 2020 the 700 MHz band will get in use for mobile phone communication (European Commission [24, 25]). It is not unlikely that by that time real-time measurements can be performed in that band. Moreover, in the U.S. the 600 MHz is planned to be used for the same purpose [26], and there are GPR systems commercially available that can already measure real-time in this band.

2.9. Conclusions and future work

We used interferometry by auto-correlation to generate and analyze monostatic, or zero-offset, numerical data from recordings of noise data generated by random-noise sources in the air that reflect in two different damaged pavement models. In one model the background medium parameters varied along one dimension and in the other model they varied in two directions, but in both models the damage was modeled as a 2D zone. Both models provided reflections that can be

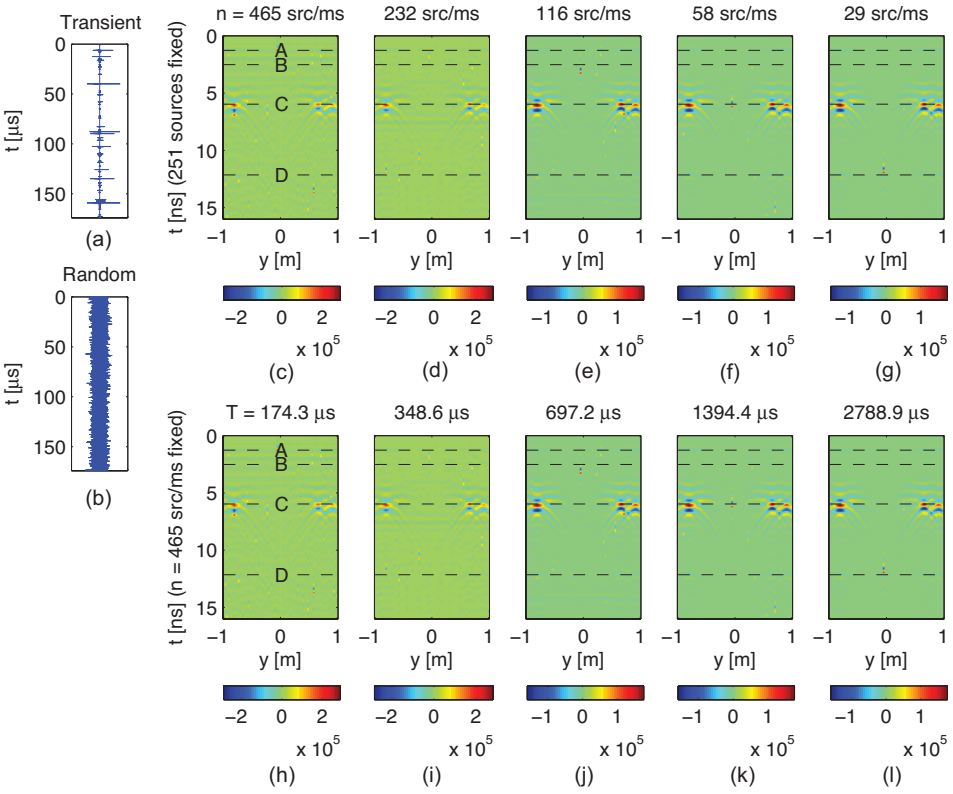

Figure 2.11: (a) Transient noise spectrum. (b) Random noise spectrum. (c-g) Analysis of the influence of the source concentration n for the case of transient sources in number of sources per millisecond (src/ms). (h-l) The influence of the measure time T with constant transient source concentration n = 465 src/ms.

used for pavement damage inspection, i.e. the same information as with a conventional mono-static B-scan could be retrieved (Figures 2.5 and 2.8). Only in detail the 2D heterogeneous model shows slightly better results than the 1D model (Figures 2.3 and 2.7). The 1D heterogeneous model is therefore recommended. Regarding the noise and pavement models we used, the concept of non-destructive pavement damage inspection by autocorrelating mono-static GPR noise data seems realistic. The source distribution, measure time, and time spreading of the noise sources only influence the interferometric result to a limited extent.

The next step is to validate this concept with actual noise recordings in the field. For practical reasons, it might be valuable to reduce the used source span-width.

References

[1] R. Feld, E. C. Slob, and J. W. Thorbecke, *Non-destructive pavement damage inspection by mono-static GPR without transmitting anything,* Geophysical Journal International (2016).

[2] C. A. Rodeick, *Roadbed void detection by ground penetrating radar,* Highway and Heavy Construction **127**, 60 (1984).

[3] K. R. Maser, *Detection of progressive deterioration in bridge decks using ground penetrating radar,* in *Experimental assessment of the performance of bridges: Proceedings of the American Society of Civil Engineers/ Engineering Mechanics Division Specialty Conference* (1986) pp. 42–57.

[4] N. S. Parry and J. L. Davis, *GPR systems for roads and bridges,* Geological survey of Finland, Special paper 16 , 247 (1992).

[5] J. Hugenschmidt, M. N. Partl, and H. de Witte, *GPR inspection of a mountain motorway in switzerland,* Journal of Applied geophysics **40**, 95 (1998).

[6] T. Saarenketo and T. Scullion, *Road evaluation with ground penetrating radar,* Journal of Applied Geophysics **43**, 119 (2000).

[7] K. Maser and T. Scullion, *Automated pavement subsurface profiling using radar: Case studies of four experimental field sites,* Transportation Research Record **1344**, 148 (1992).

[8] F. Tosti, A. Benedetto, and A. Calvi, *An effective approach for road maintenance through the simulation of GPR-based pavements damage inspection,* in *International journal of pavements conference, IJPC Paper 124-1* (São Paulo, Brazil, 2013) pp. 1–9.

[9] A. Benedetto, F. Tosti, L. Pajewski, F. D'Amico, and W. Kusayanagi, *FDTD simulation of the GPR signal for effective inspection of pavement damages,* in *Proceedings of the 15th International Conference on Ground Penetrating Radar* (IEEE, ISBN: 978-1-4799-6789-6, 2014).

[10] G. T. Schuster, *Seismic interferometry* (Cambridge university press, ISBN 978-0-521-87124-2, 2009).

[11] K. Wapenaar, D. Draganov, R. Snieder, X. Campman, and A. Verdel, *Tutorial on seismic interferometry: Part 1 - Basic principles and applications,* Geophysics **75**, 75A195 (2010).

[12] K. Wapenaar, E. Slob, R. Snieder, and A. Curtis, *Tutorial on seismic interferometry: Part 2 - Underlying theory and new advances,* Geophysics **75**, 75A211 (2010).

[13] E. Slob, D. Draganov, and K. Wapenaar, *Interferometric electromagnetic Green's functions representations using propagation invariants,* Geophysical Journal International **169**, 60 (2007).

[14] L. Liu and K. He, *Wave interferometry applied to borehole radar: Virtual multi-offset reflection profiling,* IEEE Transactions on Geoscience and Remote Sensing **45**, 2554 (2007).

[15] E. Slob and K. Wapenaar, *Practical representations of electromagnetic interferometry for GPR applications: a tutorial,* Near Surface Geophysics , 391 (2008).

[16] E. Slob and K. Wapenaar, *Electromagnetic Green's function retrieval by cross-correlation and cross-convolution in media with losses,* Geophysical Research Letters **34** (2007).

[17] R. Feld and E. Slob, *GPR without a source by use of interferometry by multi-dimensional deconvolution,* in *SEG-2014-1254: Society of Exploration Geophysicists conference* (Denver Colorado, USA, 2014) pp. 844–849.

[18] R. Snieder, K. Wapenaar, and K. Larner, *Spurious multiples in seismic interferometry of primaries,* Geophysics **71**, SI111 (2006).

[19] A. Giannopoulos, *Modelling ground penetrating radar by GprMax,* Construction and Building Materials **19**, 755 (2005).

[20] Matlab, *R2013a (8.1.0.604), 64-bit (maci64)* (The MathWorks Inc., 2013).

[21] M. J. M. Verhagen, *Strategische nota mobiele communicatie en beschikbaar stellen 800 MHz band voor mobiele breedband*, Tech. Rep. (Ministry of economic affairs in The Netherlands, http://www.rijksoverheid.nl/bestanden/documenten-en-publicaties/kamerstukken/2010/12/10/strategische-nota-mobiele-communicatie-en-beschikbaar-stellen-800-mhz-band-voor-mobiel-breedband/10184648.pdf, 2010).

[22] Antennebureau, *The information agency of the Dutch government concerning antennas*, Tech. Rep. (http://www.antennebureau.nl/onderwerpen/algemeen/veldsterktemetingen, website kept up-to-date).

[23] R. Feld and E. C. Slob, *Line-array GPR monitoring without transmitting anything,* IEEE Journal of Selected Topics in Applied Earth Observations and Remote Sensing (submitted).

[24] EU, *Radio spectrum: Pascal Lamy presents his report to the Radio spectrum: Pascal Lamy presents his report to the Commission*, Tech. Rep. (European Commission, Press Release, Brussels, 2014).

[25] EU, *Commission proposes to boost mobile internet services with high-quality radio frequencies*, Tech. Rep. (European Commission, Press Release, Brussels, 2016).

[26] T. Wheeler, *Leading towards Next Generation "5G" Mobile Services*, Tech. Rep. (FCC, https://www.fcc.gov/news-events/blog/2015/08/03/leading-towards-next-generation-5g-mobile-services, 2015).

3

Line-array GPR monitoring: virtual source data reconstruction from possible experimental configurations

Creating virtual sources at locations where physical receivers have measured a response is known as interferometry. Replacing physical sources by virtual sources at physical receiver locations is feasible using cross-correlation and deconvolution techniques. In theory interferometry requires a large receiver span width and the data must be properly sampled. To apply the method to 3D wavefields measured along a single line a 3D-to-2D wavefield transformation is necessary. We show that for measured line data this transformation leads to the largest error, which decreases with increasing offset. The method still retrieves the desired reflection response with some phase and amplitude errors. For media with small loss factors the correlation method is preferred when phase is the most important aspect in the result. The deconvolution method is in general the preferred method even when the data is undersampled. The accuracy with a virtual source might be lower than using a real source, but the result is still interpretable, with the advantages of fixed virtual source locations and orientations, while the actual sources can be changing for subsequent measurements, removal of temporal variations in the overburden, simpler setup, and lower operational costs. These results indicate that the method is worthwhile to be tested on actual measured data.

Parts of this chapter have been submitted to IEEE Journal of Selected Topics in Applied Earth Observations and Remote Sensing [1].

3.1. Introduction

For many years seismic interferometry is known for its usability in signal retrieving [2, 3]. Seismic interferometric methods create a virtual source on the position of a physical receiver. No information about the actual source is needed. Nowadays, there are different interferometric techniques available. One way is known as the cross-correlation method. Slob et al. [4] investigated the effect of the necessary approximations when cross-correlation would be used for ground-penetrating radar (GPR). They concluded that the high-frequency approximation and the assumption of wave energy conservation in the media can cause amplitude errors. Liu and He [5] applied the cross-correlation method to synthetic as well as field cross-hole radar tomography data. They demonstrated that this is advantageous for characterizing certain kinds of subsurface features. Another interferometric technique is the interferometry by deconvolution method (IbD). Wapenaar et al. [6] explored this technique for seismic waves and diffusive electromagnetic fields. The strength of this method is its usability in dissipative media. In a numerical simulation Wapenaar et al. [6] removed the air/sea interface and the direct field in controlled source electromagnetic data by use of IbD. Slob [7] studied the deconvolution method specifically for active source GPR data. He provided a general derivation in 3D, and a 2D numerical simulation for a 1D layered model for the ideal case in which there are no limitations for sources and receivers. Recently Li et al. [8] studied the possible application of passive interferometry by cross-correlation for LNAPL monitoring purposes. They modeled noise sources in 2D and concluded that LNAPL monitoring using interferometry by cross-correlation is feasible. They used a 2D model, properly sampled data, and noise sources above and below the receiver line.

However, in practice data is recorded in 3D even with a line configuration, the data is usually aliased, the maximum aperture is limited, and the (noise) sources are expected to be located above the receiver array only.

The novel contributions of this work are recognizing that actual data is coming from a 3D environment and investigate the effects of having line data instead of areal data, we investigate the effects of limited useful aperture of the receiver array, the effects of aliasing, and the effects of having (noise) sources only at one side of the receiver array. Sampling effects occur because there is an aperture limit that can be understood from Snell's law and because of aliasing when the distance between two adjacent receivers is too large. To accommodate the fact that line data is recorded in a 3D environment we apply a 3D to 2D transformation on the recorded line data and investigate the numerical errors involved. The effects of the limited useful aperture of the receiver array are studied to obtain an expected maximum offset for the retrieved virtual source data. The effects of aliasing are studied to obtain information on how much aliasing is tolerable in terms of accurate virtual source data retrieval.

3.2. Theory

We consider receivers in a line-configuration. The measured line data in the 3D environment must be converted to 2D data before we can apply 2D in-

terferometry. Then, the 2D data is decomposed in up- and downgoing wavefields, after which the upgoing wavefield is deconvolved by or cross-correlated with the downgoing wavefield to find the 2D reflection response as if it was generated by a virtual source. Interferometry by cross-correlation can be carried out with the data without up/down decomposition, but then time windowing is necessary. Here the decomposed data is used to compare results obtained with the cross-correlation and deconvolution methods. In this section we first describe how we transform 3D data to 2D. What follows is the theory regarding decomposition, and then interferometry in the last section.

3.2.1. 3D → 2D transformation of the line data

Through the years different methods have been proposed to transform line data measured in 3D to 2D data. Auer et al. [9] wrote a thorough article about the validity of 3D to 2D transformations. The most common approach for seismic purposes is by multiplying the time-traces with the square root of time, followed by time-convolving this with an inverse square root of time: $G_{2D} = \left(G_{3D}\sqrt{t}\right) * \frac{1}{\sqrt{t}}$, with t time [9], [10]. For GPR purposes sometimes an approximation that contains parameters estimated from the first arrivals in the data is used [11], [12]. Others make use of a ray tracing techniques to estimate these parameters [13].

Green's functions, G_{2D} and G_{3D}, in 2D and 3D, can be obtained by finite difference time-domain modeling. By taking the positions of the sources and receivers and the medium parameters of the most-upper ground layer an exact conversion factor is obtained for that configuration. The underlying assumption is that a conversion in the homogeneous space can be used in the actual configuration. Since we use all information known during an experiment, our approach should be better, or at least as good as other transformation methods. Note that this works for us, because we know the receiver and source positions in our setup precisely, and we are willing to perform 3D FDTD simulations. Any difference between the real experimental setup and our simplification will induce an error during the transformation. To find the 2D electric and magnetic field components $\hat{E}_{x,2D}$ and $\hat{H}_{y,2D}$ we do the following for each source-receiver pair,

$$\hat{E}_{x,2D} = \left[\frac{\hat{E}_{x,2D,0}}{\hat{E}_{x,3D,0}}\right]\hat{E}_{x,3D}, \tag{3.1}$$

$$\hat{H}_{y,2D} = \left[\frac{\hat{H}_{y,2D,0}}{\hat{H}_{y,3D,0}}\right]\hat{H}_{y,3D}, \tag{3.2}$$

with the hat symboling a quantity in the frequency-space domain, $\hat{E}_{x,3D}$ and $\hat{H}_{y,3D}$ represent the 3D field components from the line-configuration and subscript 0 denotes that this is the modeled data for the homogeneous case. Obviously, equations (3.1) and (3.2) are exact for a homogeneous Earth model. An error can be expected due to the Earth's inhomogeneity.

3.2.2. Decomposition of the 2D electric and magnetic fields into upgoing and downgoing wavefields

In practice the electric field strength can be measured with a GPR antenna, and the magnetic field with a loop antenna [14]. The loop detectors could be placed between the dipole antennas. By averaging their values one can get the same measurement location of the electric and magnetic fields. As alternative, the magnetic component can be calculated from the electric field, because the receivers will be assumed to be placed on a lateral locally homogeneous boundary [15], which we illustrate later in this section. After the transformation a 2D TE-mode configuration is obtained with sources and receivers in a homogeneous half space above the earth's surface. The receivers measure the horizontal electric field $\hat{E}_x$ and horizontal magnetic field $\hat{H}_y$. The horizontal electric wavefield consists of a mix of downwards and upwards propagating wavefields. This is also the case for the horizontal magnetic wavefield $\hat{H}_y$. Slob [7] assumed the decomposed upgoing and downgoing wavefields available from measurements. However, those wavefields need to be determined from the measured electric and magnetic fields. In this section we decompose the (total) downgoing and the (total) upgoing wavefields, symbolized respectively by $\hat{P}^+$ and $\hat{P}^-$, from the electric and magnetic wavefields $\hat{E}_x$ and $\hat{H}_y$. Figure 3.1 summarizes this schematically.

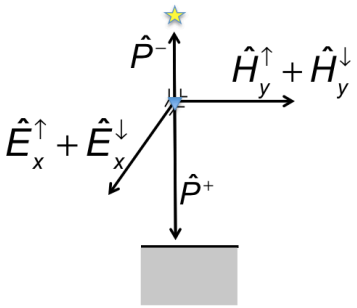

Figure 3.1: A source, symbolized by a yellow star, emits a signal consisting of the horizontal electric $\hat{E}_x$ and magnetic $\hat{H}_y$ fields. This signal reflects at an interface, presented here as a horizontal bar. Then it is received at the position symbolized by a blue triangle. The record is decomposed in upgoing (-) and downgoing (+) propagating wavefields $\hat{P}$, which will be used to retrieve the reflection response.

We choose the electric field $\hat{E}_x$ for the upgoing and downgoing wavefields $\hat{P}^-$ and $\hat{P}^+$ in frequency-space domain,

$$\hat{E}_x = \hat{P}^+ + \hat{P}^-. \tag{3.3}$$

We define $\zeta = j\omega\mu$, with j the imaginary unit, ω the angular frequency and μ the magnetic permeability, and ∂_z as the vertical partial derivative. Using the Maxwell-Faraday equation for the magnetic field $\hat{H}_y$ holds:

$$\hat{H}_y = -\frac{\partial_z \hat{E}_x}{\zeta}. \tag{3.4}$$

The receivers are placed on a lateral locally homogeneous boundary. Therefore the decomposition can also be done in the frequency-wavenumber domain. Let us use a diacritical tilde to indicate a quantity in the frequency-wavenumber domain. The horizontal electric field $\tilde{E}_x$ and the horizontal magnetic field $\tilde{H}_y$ can be written as,

$$\tilde{E}_x = \tilde{P}^+ + \tilde{P}^-, \tag{3.5}$$

$$\tilde{H}_y = \frac{\Gamma_0}{\zeta}\left(\tilde{P}^+ - \tilde{P}^-\right), \tag{3.6}$$

with $\Gamma_0 = \sqrt{k_y^2 + \eta\zeta}$ and $\eta = j\omega\epsilon + \sigma$, in which k_y symbolizes the horizontal wavenumber, ϵ the permittivity and σ the conductivity. Therefore the up/downgoing waves $\tilde{P}^+$ and $\tilde{P}^-$ are:

$$\tilde{P}^+ = \frac{1}{2}\left(\tilde{E}_x + \frac{\zeta}{\Gamma_0}\tilde{H}_y\right), \tag{3.7}$$

$$\tilde{P}^- = \frac{1}{2}\left(\tilde{E}_x - \frac{\zeta}{\Gamma_0}\tilde{H}_y\right). \tag{3.8}$$

Because we know the electric and magnetic properties at the receiver level we can carry out this decomposition. Slob [7] and Li et al. [8] assumed that the up/downgoing waves can be determined perfectly in the frequency-wavenumber domain. In section 3.4 we evaluate the effects of this assumption.

Here, we described how electric and magnetic field-data of a line configuration in a 3D world can be converted to 2D field-data, followed by how these field-data can be decomposed in upgoing and downgoing wavefields. In the next section the reflection response will be retrieved from these decomposed wavefields.

3.2.3. Retrieving the reflection response from the upgoing and downgoing wavefields

Although the receivers are placed on a lateral locally homogeneous boundary, the subsurface below the receiver-level is heterogeneous. Therefore, we need to continue in the frequency-space domain. The upgoing wavefield $\hat{P}^-$ is the convolution between the downgoing wavefield $\hat{P}^+$ and the reflection response $\hat{R}$,

$$\hat{P}^-(y_r, y_s, \omega) = \int_{y\in\partial\mathbb{D}} \hat{R}(y_r, y, \omega)\,\hat{P}^+(y, y_s, \omega)\,d^2y. \tag{3.9}$$

In theory, the integration variable y and receiver positions y_r lay on the boundary $\partial\mathbb{D}$ with an infinite aperture, and also the source positions y_s are on a boundary with infinite aperture. This is the result of the formal derivation in [7]. Note that there is only convolution in the time-domain, which is here a product in frequency domain. In space-domain it is not a real spatial convolution, but absolute position is important, because of subsurface heterogeneities. Only when the surface would be laterally homogeneous we could perform this step separately for each plane wave component, i.e. division in wavenumber-frequency domains, but that does

not apply to our case. Under certain conditions this equation can be used for non-horizontal boundaries [16]. However, in this paper we consider the effects of a finite aperture and the effects of aliasing (i.e. too much distance between the individual receivers).

Cross-correlating (3.9) with $\left(\hat{P}^{+}\left(y', y_{s,i}, \omega\right)\right)^{*}$, where the star symbolizes complex conjugation, for arbitrary point y' on both sides, and summing over all N_s source signals, gives

$$\sum_{i=1}^{N_s} \hat{P}^{-}\left(y_r, y_{s,i}, \omega\right)\left(\hat{P}^{+}\left(y', y_{s,i}, \omega\right)\right)^{*} = \sum_{i=1}^{N_s} \int_{y\in\mathbb{D}} \hat{R}\left(y_r, y, \omega\right) \hat{P}^{+}\left(y, y_{s,i}, \omega\right) d^2 y \left(\hat{P}^{+}\left(y', y_{s,i}, \omega\right)\right)^{*}, \quad (3.10)$$

which is similar to what is given in [17].

In the discrete version of equation (3.9) the first variable between brackets of each quantity corresponds to different rows of a matrix, and the second variable to different columns. In matrix notation this matrix multiplication is

$$\hat{\mathbf{P}}^{-} = \hat{\mathbf{R}}\hat{\mathbf{P}}^{+}, \quad (3.11)$$

so that

$$\hat{\mathbf{R}} = \hat{\mathbf{P}}^{-}\left[\hat{\mathbf{P}}^{+}\right]^{-1}, \quad (3.12)$$

where $\left[\hat{\mathbf{P}}^{+}\right]^{-1}$ is the inverse of $\hat{\mathbf{P}}^{+}$ and there is summation over the sources during matrix-multiplication. When there are more sources than receivers, the matrix is overdetermined. Then the least-square error solution is a good choice:

$$\hat{\mathbf{R}} = \hat{\mathbf{P}}^{-}\left(\hat{\mathbf{P}}^{+}\right)^{\dagger}\left[\hat{\mathbf{P}}^{+}\left(\hat{\mathbf{P}}^{+}\right)^{\dagger} + \epsilon\,\hat{\mathbf{I}}\right]^{-1}, \quad (3.13)$$

with ϵ a positive real number for stabilization and $\hat{\mathbf{I}}$ the identity matrix. The symbol $\dagger$ denotes the conjugated transpose of the matrix. Note the similarities with the integral notation (3.10) for $\epsilon = 0$. After multiplication of the reflection response with the source-wavelet, the virtual source reflection response is retrieved from the measured data. This method is the least-squares solution of *interferometry by deconvolution* (IbD) [7].

When there are fewer sources than receivers the solution can be obtained using a minimum norm solution:

$$\hat{\mathbf{R}} = \hat{\mathbf{P}}^{-}\left[\left(\hat{\mathbf{P}}^{+}\right)^{\dagger}\hat{\mathbf{P}}^{+} + \epsilon\,\hat{\mathbf{I}}\right]^{-1}\left(\hat{\mathbf{P}}^{+}\right)^{\dagger}. \quad (3.14)$$

There are anyway cut-off phenomena that cause errors in the result. To provide each receiver with the same bandwidth as the sources, all receivers require the same aperture of sources.

Equation (3.13) constructs the reflection response from a virtual source at a receiver position, without the direct field, by using only received data and information about the immediate surroundings of the receivers. Huygens' principle says that each point on the wavefront behaves as a point source, and likewise with interferometry we reduce the wave-front to such a point source.

An alternative for the least-square like inversion is by constructing a pseudo-inverse by use of singular value decomposition [18]. Both methods were tested for our situation of controlled sources and the least-square inversion was found to be faster and notably more precise than the pseudo-inverse. For the case of uncontrolled sources the pseudo-inverse seems to work better [19], but this discussion goes beyond the scope of this paper. We continue by introducing the effects of too much distance between individual receivers and the effects of the finite aperture. The first is important because of the Nyquist criterium for the Fourier transformation, and the latter for the sampling of the spectrum.

Effects of too much distance between individual receivers

The integration variable y in equation (3.9) corresponds to the virtual source position y. The virtual source position y and receiver position y_r are the same in the discrete case. Note that the distance dy between receivers needs to be sufficiently small for the discretized version (3.11) to represent equation (3.9). In practice, dy is restricted to the physical size of the receivers, because these need to be placed next to each other. Further, taking more distance between the individual receivers means that less receivers are required. Its effects on the response retrieval is important for practical decisions about the most beneficial receiver configuration, given the antennas that are available. In this work we increase dy and consider its effects on the retrieved reflection response. This part is illustrated in paragraph 3.4.3.

Effects of finite aperture

In the theory the amount of sources and receivers is infinite, covering an infinite span width. This is not realizable in a practical setup. Due to a finite amount of receivers the integrals become finite summations. Therefore the boundaries at the end of the receiver array introduce artifacts. Figure 3.2 shows schematically the expected position of this cut-off clutter. Likewise, also the finite source-array causes clutter.

When using interferometry by deconvolution the finiteness of the receiver array is expected to cause clutter behind the reconstructed signal. The wider the span of receivers, the longer the time span of a signal that can be retrieved, without effects of the finite boundaries. This is because the interaction at the most furthest receivers is physical, and hence the information that comes from the endpoints of the array needs more time to travel for wider receiver arrays. We use a time-window that is short enough, so that this cut-off clutter falls outside the window. This discussion is continued in paragraph 3.4.3.

When the term $\hat{\mathbf{P}}^{+}\left(\hat{\mathbf{P}}^{+}\right)^{\dagger}$ of equation (3.13) would be taken as a diagonal matrix

with constants on its diagonal, the reflection response $\hat{R}$ can be expressed as:

$$\hat{\mathbf{R}} \sim \hat{\mathbf{P}}^{-}\left(\hat{\mathbf{P}}^{+}\right)^{\dagger}\left|\widehat{W}\right|^{-2}, \tag{3.15}$$

with $\widehat{W}$ the source signal. This is the reflection response $\hat{R}$ according to *interferometry by cross-correlation* (CC). In the case of CC the limited amount of sources will create non-physical events, ideally before the first arrival [20]. As mentioned, there is summation over the sources during matrix-multiplication. Also in equation (3.15) there is a sum over the sources. This also holds for IbD (3.13), but there all receivers are required due to the matrix-inversion. For CC the correlation can be performed for each individual receiver-pair. Then the finite receiver array does not cause problems. However, the finite source array can cause problems. The sources at infinite distance from the receiver pair will form a stationair point during the CC process, which results in non-physical events at $t = 0$. In the case of a finite source array there is a travel-time difference between a source and a receiver, and the same source with another receiver. Therefore non-physical events arrive just before or just after $t = 0$, depending on which receiver-data you reverse in time.

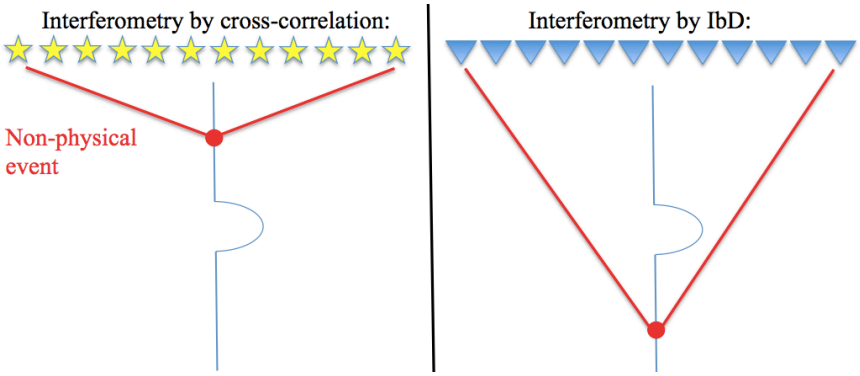

Figure 3.2: Schematic position of the clutter (shown as red dot) induced by the endings of the array.

3.3. Simulation model

In a 10 x 10 x 3 m^3 container of sand, several objects have been buried. One of these objects is a 1.85 m long metal pipe with a diameter of 9 cm, and conductivity 10^7 S/m, that lays horizontally at 0.5 m depth [21]. The sand is assumed homogeneous with frequency independent properties, a relative electric permittivity of $\varepsilon_r = 3.1$ and a conductivity of $8 \cdot 10^{-4}$ S/m [21]. This simple configuration is a good example because the method and our approximations do not depend on the complexity of the subsurface as long as there is a subsurface scattering object. The parameters are implemented using 2D and 3D Finite Difference Time-Domain (FDTD) codes (GprMax [22]). The perfectly matched layer boundaries of the finite grid have been optimized by comparing the simulation with a much larger grid. The grid size has been optimized by investigating the effect of different grid sizes on

the final result. Figure 3.3 sums up the information schematically with a drawing of the cross-section.

In the model, sources subsequently emit a Ricker wavelet with a center frequency of 900 MHz. Unshielded receivers are placed 2 cm below the earth's surface. In this way they are in complete contact with the medium. Without loss of generality, the receivers are assumed to be lossless, non-reflecting point receivers. To represent receivers as point receivers is sufficient for a numerical study of an experimental setup used to validate interferometry applied to GPR. The only difference with a physical receiver would be a filter-effect, including for instance the strong coupling to the incident EM fields, but the theory of the numerical validation does not depend on that. Numerical work shows that 70 receivers spread over 2.84 m, with 4 cm between two adjacent receivers, are necessary to retrieve an accurate result with the IbD procedure, see Figure 3.3 for the schematic drawing of this setup. However, this is not always practical and a measurement setup with less receivers is desired from a practical point of view. Small receiver spacing is especially not practical when one thinks ahead to a setup with receivers organized in a plane, where the necessary amount of receivers will be much larger. In paragraph 3.4.3 alternative configurations are considered.

Consider the case of a ray nearly parallel to the surface in air that enters a medium with relative permittivity ε_r and temporarily assume that the effects of conductivity can be neglected. Then Snell's law reduces to the following expression of the critical angle θ_{crit}:

$$\sin\theta_{crit} = \frac{1}{\sqrt{\varepsilon_r}}. \tag{3.16}$$

The critical angle θ_{crit} is the angle with respect to the normal, in which a horizontally traveling ray can bend when it enters the medium (see Figure 3.3). All other rays will enter the medium with a smaller angle. For this reason only rays crossing a certain area of the interface can reach the object in the ground [7], while a real source at a physical receiver's location below the surface would not be limited. Note that the difference with [7] is that here we have a pipe as scattering object instead of only horizontal layers and hence the upgoing wavefield is not restricted in spatial bandwidth. All sources generate waves that reach the pipe and its reflection is recorded by every receiver. Therefore, the zone where virtual sources can be created is limited, but the receivers are useful at any position. Here, we will consider a virtual source in the middle. We desire accurate IbD data from all receivers to construct the response with respect to the virtual source in the middle. For the situation described in this section, the critical angle θ_{crit} is 34.6^o. Looking at the surface, the range on the surface from which rays can reach the object is less than 0.78 m long. Less, because the critical angle is an overestimation, since the source aperture is finite. This range is marked red in Figure 3.3. It means that the part of the downgoing wavefield that misses the red line will miss the object. Hence, the downgoing wavefield outside the red district will not contribute to any reflection. However, the wavefield that does reach the object can reflect to receivers outside the red marked area, due to the cylindrical shape of the pipe. The data coming from receivers outside the marked district seems to be essential for the reduction

of cut-off clutter.

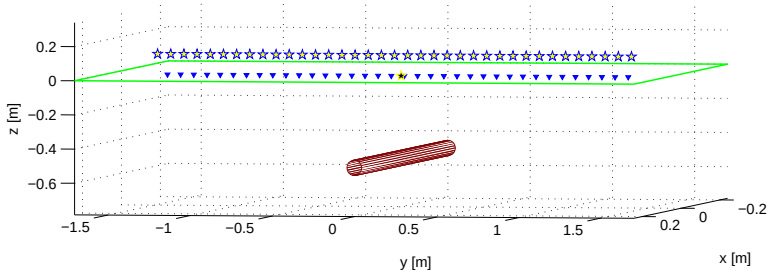

(a) Schematic display of the setup

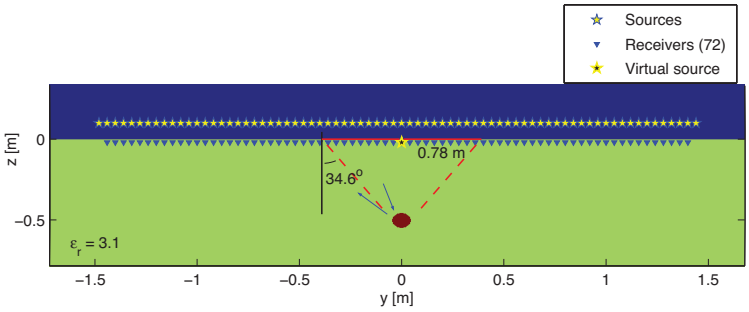

(b) Schematic front-view of the setup

Figure 3.3: All sources will generate a wavefield that reaches the pipe by passing the triangular domain indicated in red. All receivers will measure a reflection from the pipe from any sources.

3.4. Numerical results

GprMax3D considers media with frequency independent and isotropic properties. The setup schematically shown in Figure 3.3 has been simulated, with a grid size of one-twentieth of the minimum wavelength. Also the 'ideal' case of a source at the virtual source position in the middle of the receiver array has been simulated (see Figure 3.3 for the virtual source position). For results, only numerical data of receivers in the red marked area are shown. Outside the red zone it is not useful to create virtual sources, because these would not generate waves that will 'see' the pipe (as explained in the previous section).

3.4.1. 3D → 2D transformation of the line configuration

Figure 3.3 shows the geometry. However, normally only the source and receiver positions and the medium parameters at the surface are known in advance. Therefore, we assume the situation as drawn in Figure 3.4, in which the subsurface is a homogeneous medium. Using equations (3.1) and (3.2) the 3D electric and magnetic field components are transformed to 2D data: $E_x(t)$ and $H_y(t)$. Least-square

type optimalisation like in equation (3.13) is used. In Figures 3.5 and 3.6 the transformed field components are compared with the ideal 2D field components. The 'ideal output' is the result of 2D modeling. Figure 3.5 shows this comparison for the electric component $E_x(t)$ and Figure 3.6 for the magnetic component $H_y(t)$. Figures 3.5a and 3.6a show the comparison with respect to the middle source. The transformation causes respectively 40 and 62 percent error, based on comparison of the maximum absolute amplitudes after 6 ns. Figures 3.5b and 3.6b show the comparison with respect to the outermost source, which is the source that is the farthest from the middle source. For this case the errors are respectively 25 and 15 percent. The error has the shape of the reflected wave, because the reflecting object is the only inhomogeneity in our Earth model.

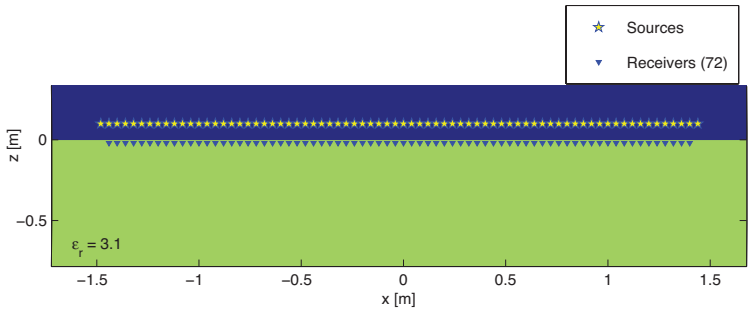

Figure 3.4: Information used for the 3D → 2D transformation: source and receiver positions and medium parameters of the surface. The world below the surface is assumed homogeneous. Receivers are assumed to be lossless, non-reflecting point-receivers.

3.4.2. Decomposition of the 2D electric and magnetic fields into upgoing and downgoing wavefields

First, the electric and magnetic field components are transformed to 2D data. Then, this 2D data is decomposed in up- and downgoing wavefields, using equations (3.7) and (3.8). Note that those equations require the field components at the exact same time and position. Figure 3.7 shows these decomposed wavefields for the 2D data at two different receiver-positions. For comparison, it also shows the decomposed wavefields for the case that the transformation to 2D would have been ideal. The direct wave is transformed perfectly. The error in the reflected wave is caused by the error in the 3D to 2D transformation.

3.4.3. Retrieving the reflection response from the upgoing and downgoing wavefields

Then, interferometry by deconvolution (IbD) is applied, using equation (3.13). The result is shown in Figure 3.8a. The stabilization factor $\in$ is chosen to be frequency dependent, but independent of the receivers. Last, but not least, interferometry by cross-correlation (CC) is done, using the decomposed wavefields as described in equation (3.15). The result can be seen in the same Figure 3.8a. Its amplitude is

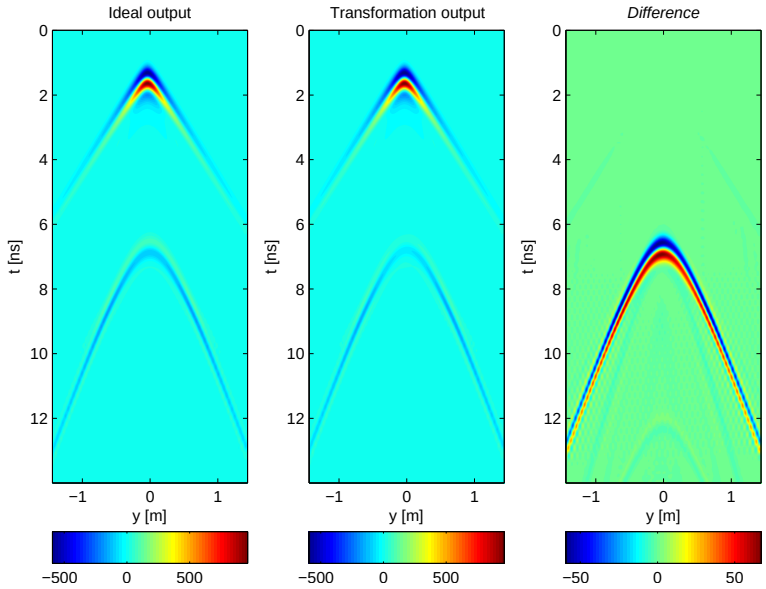

(a) Transformed $E_x(t)$ w.r.t. central source

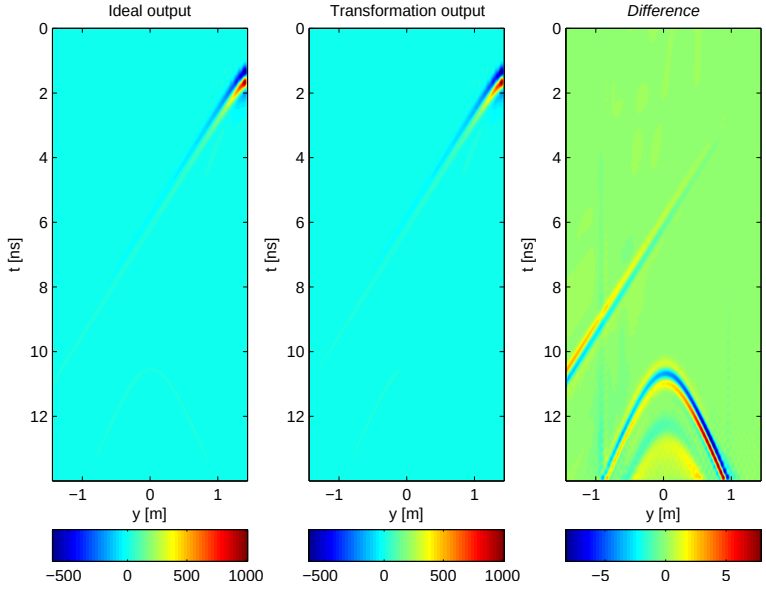

(b) Transformed $E_x(t)$ w.r.t. outermost source

Figure 3.5: The transformed electric field components are compared with the ideal 2D output, with respect to the central source and to the outermost source. Also the difference between the transformed output and the ideal output are shown.

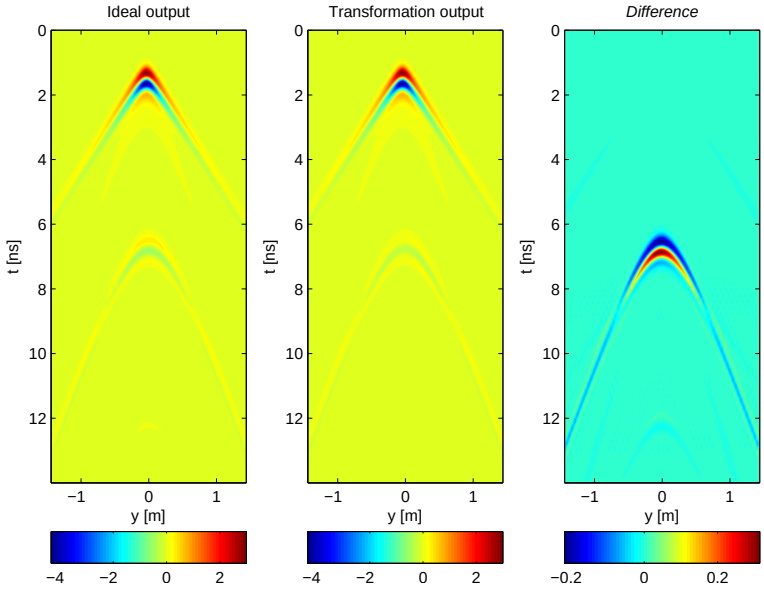

(a) Transformed $H_y(t)$ w.r.t. central source

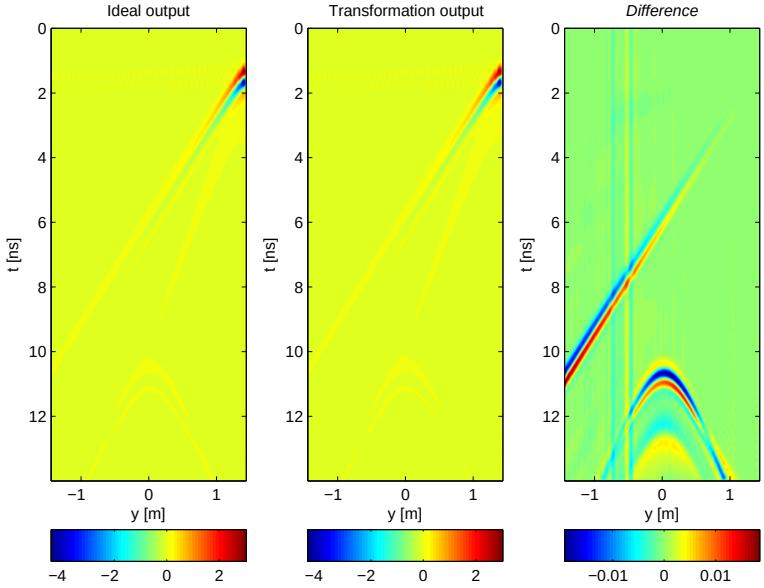

(b) Transformed $H_y(t)$ w.r.t. outermost source

Figure 3.6: The transformed magnetic field components are also compared with the ideal 2D output, with respect to the central source and to the outermost source. Also the difference between the transformed output and the ideal output are shown.

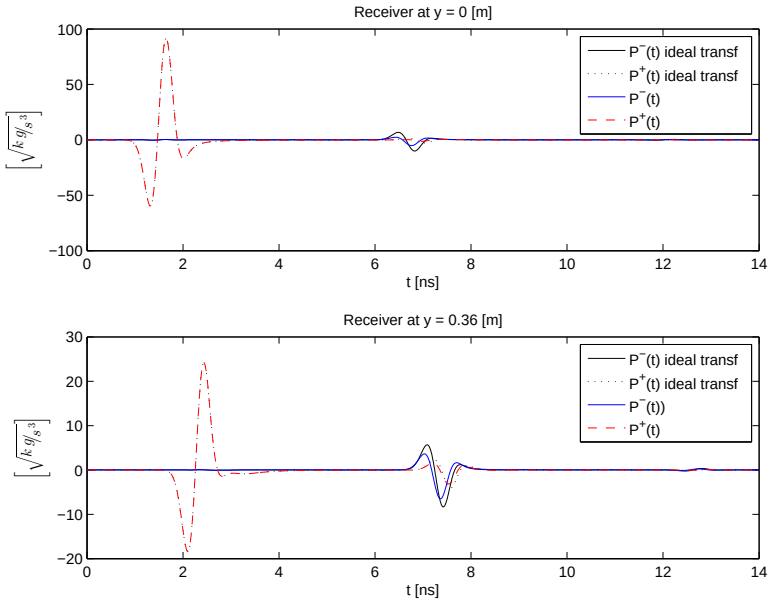

Figure 3.7: Decomposition: up- and downgoing wavefield at y = 0 m and y = 0.36 m, both w.r.t. a source at y = 0 m. The decomposed waves are compared with the case in which the 3D → 2D transformation went perfectly.

scaled by a constant factor such that it matches the ideal results. The 'ideal output' is determined by simulating a source on the virtual source's position in 2D. In Figure 3.8b the amplitudes of all the mentioned results are shown for comparison at two different offsets.

The IbD result method yields correct amplitude information by itself, whereas the CC result does not and is scaled. Close to the center receivers IbD deviates more from the ideal output, probably caused by the 3D to 2D transformation, while the more outer receivers that are still trustable (see section 3.3) and match better with the ideal result. IbD gives reasonable amplitude information at those receiver positions. The IbD result seems to show some more clutter than the CC output.

Note the non-physical event of the cross-correlation result. There are flares in the result, because the right formulation assumes the normal component on the surface. This means a multiplication of the cosine with the angle approaching 90 degrees at large offsets, so that the contribution of those sources become zero at the surface. However, the locations of the sources are unknown and therefore we cannot determine this cosine and make it 1. All sources at large horizontal distance are in this stationary area and contribute, causing the flares: it are evanescence waves that are added incorrectly. The CC result does not completely overlap with the ideal output, because the non-physical event coincides with the first peak. The CC output shows the reflection of the earth's surface, while with IbD the earth's surface and everything else above the receiver array is homogenized, although

some clutter can be seen there in the IbD output. If this is not a problem and the user is interested in phase information only, then the CC method should be used. Note that the CC method neglects dissipation and therefore applies to low-dissipative Earth models, like the one we consider, whereas IbD would be able to deal with dissipative media. The pipe is a strong reflector, and that is probably why CC is not negatively affected by the single-sided illumination. The reflector could then function as a cylindrical mirror, taking count for the side without sources.

When IbD is applied directly to 3D data, without transforming it to 2D first, then the output is strongly affected by one or more additional reflections. Even the shape of the reflected wave from the pipe looks worse, than with transformation. Also for the case that CC is applied directly to 3D data the output looks less stable than with transformation in advance. These results are not shown here.

Effects of too much distance between individual receivers

Figure 3.8 shows the results for the case that 72 receivers are spread over almost 3 m, with a distance of 4 cm between each two receivers. For practical purposes it is necessary to look for configurations with a larger distance between each two receivers and a smaller amount of receivers. In order to protect the receiving antenna from the environment, without shielding, the covering or protecting material must be an epoxy raisin or other non metallic cover. Two other configurations are considered: 48 receivers spread over 2.82 m, and 36 receivers over 2.80 m. Figure 3.9a shows the corresponding IbD outputs and compares them with the ideal output, the case that IbD is applied to a configuration with 70 receivers with 4 cm spacing and the same case assuming the transformation 3D $\rightarrow$ 2D can be done without error. A closer look is given in Figure 3.9b, where the same comparison is shown for two specific receivers.

It is clear that less data due to less receiving antennas gives a result with more clutter. An important observation is that the transformation 3D $\rightarrow$ 2D seems to cause most of the error. The error due to reducing the number of receivers is relatively small, considering that the amount of received data is halved. The aliasing criterion for the reflected wave is much weaker than for the direct wave, because the propagation of the direct wave has a downward component reducing the horizontal component of the wave slowness.

Figures 3.10a and 3.10b show the same comparison, but now with the analysis performed using interferometry by cross-correlation.

The wavefields are curved most near the central receiver. Further from the center the data is more linear. The reason why it becomes linear is the spatial bandwidth limitation due to the critical angle or maximum angle of the finite source aperture. It may seem logical to reduce the amount of receivers further by non-linear interpolation between receivers on a non-linear grid spacing [23]. Analysis of this procedure shows that using non-linear interpolation adds data that tends to cause clutter in the results. There might exist a non-linear configuration that is better than the linear configuration we use here, but finding it is not trivial.

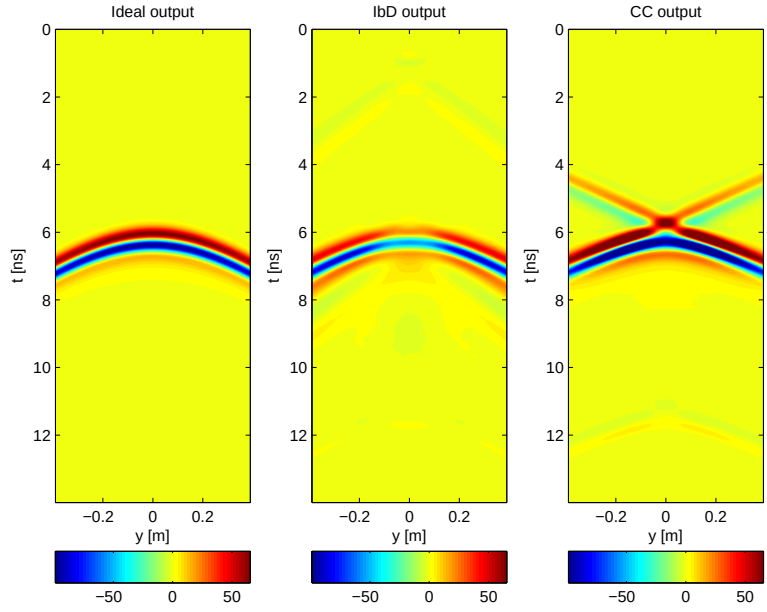

(a)

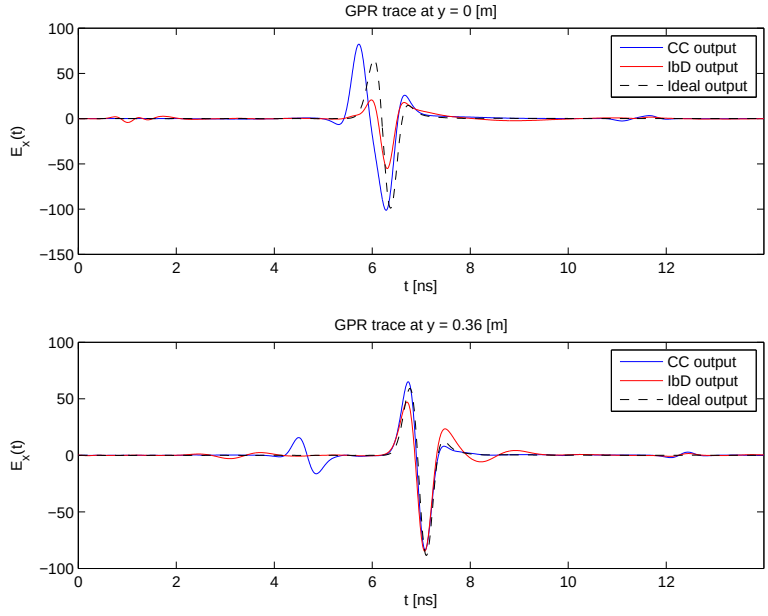

(b) Cross-section at two different offsets

Figure 3.8: Comparison of the response after a virtual source created by interferometry by deconvolution (IbD) and interferometry by cross-correlation (CC) with the case of a real source on this position (ideal case).

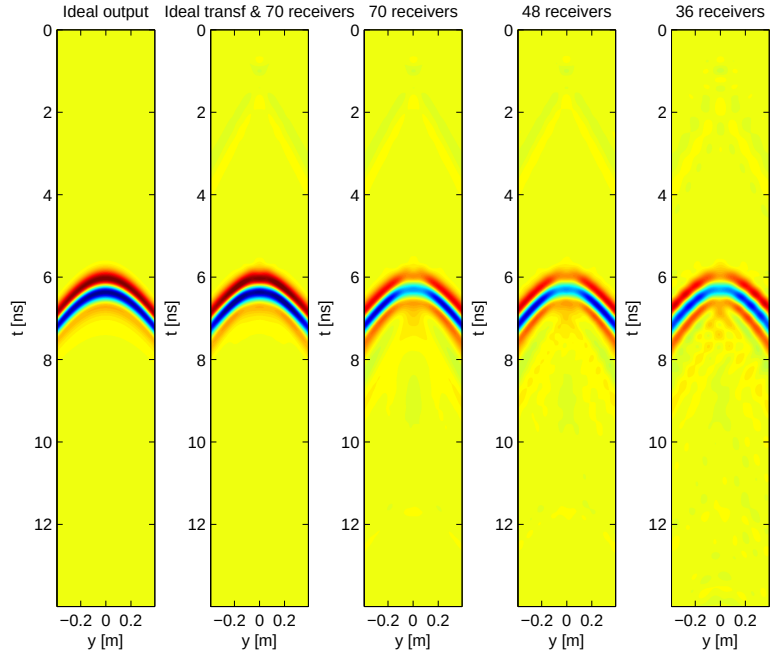

(a)

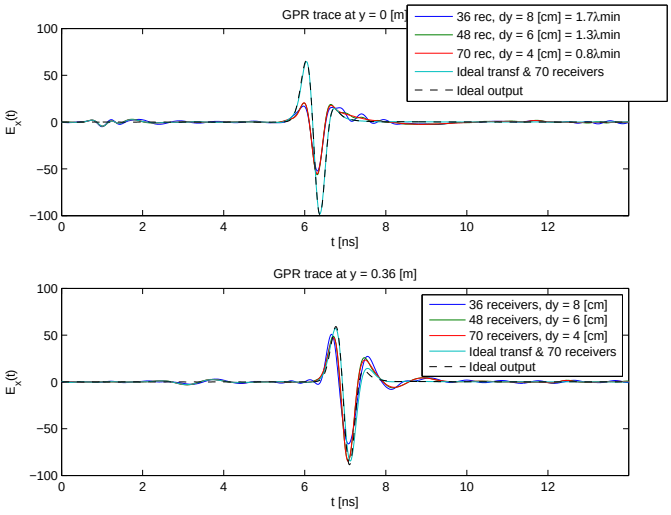

(b) Cross-section at two different offsets

Figure 3.9: Comparison of the response after a virtual source created by IbD using data of different configurations existing of different receiver amounts (with different inner distances expressed in the smallest wavelength): 70 ($0.8\lambda_{min}$ = 4 cm), 48 ($1.3\lambda_{min}$ = 6 cm) and 36 ($1.7\lambda_{min}$ = 8 cm). The 70 receivers configuration is also considered for the errorless 3D → 2D transformation, and the ideal output is displayed. Fig 3.9a: All graphs are shown w.r.t. the same colorbar.

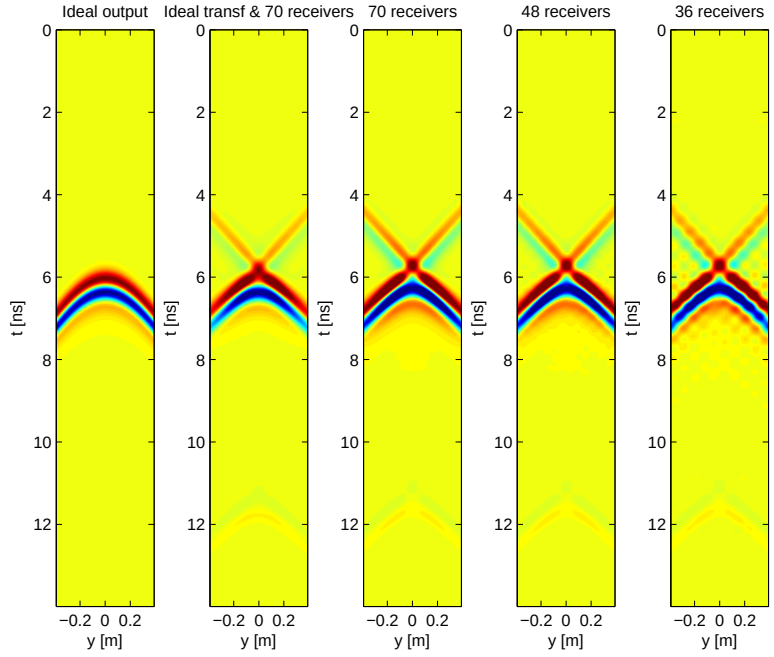

(a)

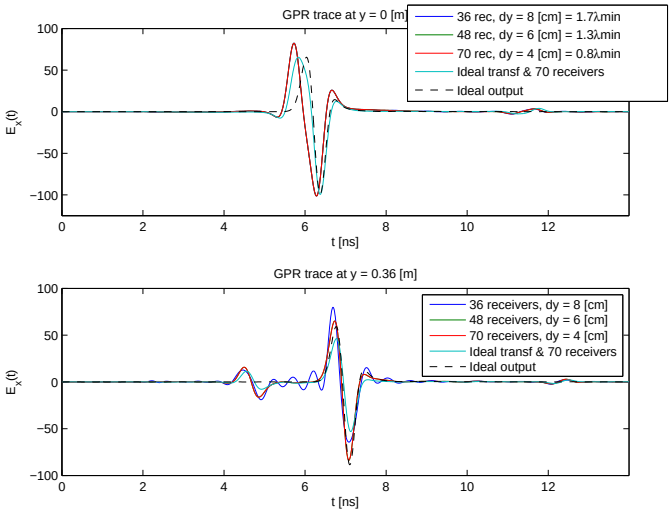

(b) Cross-section at two different offsets

Figure 3.10: Comparison of the response after a virtual source created by CC using data of different configurations existing of different receiver amounts (with different inner distances expressed in the smallest wavelength): 70 ($0.8\lambda_{min}$ = 4 cm), 48 ($1.3\lambda_{min}$ = 6 cm) and 36 ($1.7\lambda_{min}$ = 8 cm). The 70 receivers configuration is also considered for the errorless 3D → 2D transformation, and the ideal output is displayed. Fig 3.10a: All graphs are shown w.r.t. the same colorbar.

Effects of finite aperture

For the sake of the credibility of the setup used to validate interferometry by deconvolution, it is desirable to stop 'receiving' before the cut-off effects of the receiver array endings have had time to reach the marked area, so that the effect is left out of the result. However, if the measurement time is so short that the signal suddenly goes to zero, another cut-off effect will cause clutter in the result. Therefore, it is wise to stay between this minimum and maximum measurement-time. The maximum measurement-time can perfectly be extended, if it is possible to extend the receiver array. Within this time-frame we are free to choose the measurement-time. Here we are satisfied with measurements of 14 ns, also for the sake of the credibility, because it includes the reflection of the earth's surface that IbD should erase, while CC does not do this.

In the field of interferometry by cross-correlation (CC) it is common to taper the edges to reduce the cut-off effect by applying a Hanning window. The effect of this taper is that the cut-off clutter is smoothened over a larger period in time after applying IbD, but it also speeds-up this effect, i.e. it will arrive earlier in time. For the case of a limited amount of receivers this reduces the maximum measurement time undesirable. Therefore, the use of such a taper is not recommended for similar configurations and circumstances in practice.

3.5. Discussion and Conclusion

A receiver array is placed at a certain depth below the surface. Interferometry is applied to retrieve the reflection response with respect to a virtual source at one of the receiver positions, while the actual source is used at or above the surface. This gives several advantages for monitoring applications, because here it is desirable to leave receivers in the same set up for time-lapse measurements over longer timescales [8]. Then the receiver and virtual source locations and orientations are fixed and known, while the actual sources can be changing for subsequent measurements as these will be eliminated in the deconvolution or cross-correlation step. For N measurements there are N^2 virtual sources. This makes the setup much easier and reduces the operational costs. Receivers could also be placed below the groundwater table, in which case interferometry by deconvolution will remove temporal variations in the partially saturated overburden.

We have shown that 2D interferometry by deconvoluton or correlation can be carried out on line data recording 3D wavefields. The accuracy of the resulting reflection response generated by a virtual source in a line-configuration is most negatively affected by the necessary 3D-to-2D data transformation and much less by undersampling. This transformation becomes more accurate with increasing offset for which reason the near offset data is most negatively impacted. There might be more advanced 3D-to-2D transformation methods available [9] that could possibly improve the results, but the used simple method provides an interpretable output. Having sources available only on one side of the receiver array in this study does not negatively affect the correlation method. In fact the correlation method is preferred when the medium is a low-loss medium and the resulting phase information is desired over amplitude information. The GPR images with respect to virtual

sources will suffer from artifacts, but are still interpretable with the advantages mentioned earlier in this section. The modeled results show that retrieving virtual reflection responses seems feasible on real data, which is the next step toward a real world application of the technology.

References

[1] R. Feld and E. C. Slob, *Interferometric virtual source GPR data reconstruction by simulation of possible experimental line-configurations,* IEEE Journal of Selected Topics in Applied Earth Observations and Remote Sensing (2016).

[2] F. Scherbaum, *Seismic imaging of the site response using microearthquake recordings: Part I. method,* Bulletin of the Seismological Society of America **77**, 1905 (1987).

[3] M. J. Buckingham, B. V. Berkhout, and S. A. L. Glegg, *Imaging the ocean with ambient clutter,* Nature **356**, 327 (1992).

[4] E. C. Slob, D. Draganov, and C. P. A. Wapenaar, *Interferometric electromagnetic Green's functions representations using propagation invariants,* Geophysical Journal International **169**, 60 (2007).

[5] L. Liu and K. He, *Wave interferometry applied to borehole radar: Virtual multi-offset reflection profiling,* IEEE Transactions on Geoscience and Remote Sensing **45**, 2554 (2007).

[6] C. P. A. Wapenaar, E. C. Slob, and R. Snieder, *Seismic and electromagnetic controlled-source interferometry in dissipative media,* Geophysical Prospecting **56**, 419 (2008).

[7] E. C. Slob, *Interferometry by deconvolution of multicomponent multioffset GPR data,* IEEE Transactions on Geoscience and Remote Sensing **3** (2009).

[8] J. Li, Z. Zeng, E. C. Slob, X. Chen, and F. Liu, *Simulation of GPR passive interferometry using cross-correlation for LNAPL model monitoring application,* Geophysical Journal International **199**, 1919 (2014).

[9] L. Auer, A. M. Nuber, S. A. Greenhalgh, H. Maurer, and S. Marelli, *A critical appraisal of asymptotic 3D-to-2D data transformation in full-waveform seismic crosshole tomography,* Geophysics **78**, R235 (2013).

[10] E. Crase, A. Pica, M. Noble, J. McDonald, and A. Tarantola, *Robust elastic nonlinear waveform inversion: Application to real data,* Geophysics **55**, 527 (1990).

[11] N. Bleistein, *Two-and-one-half dimensional in-plane wave-propagation,* Geophysical Prospecting **34**, 686 (1986).

[12] J. R. Ernst, A. G. Green, H. Maurer, and K. Holliger, *Application of a new 2D time-domain full-waveform inversion scheme to crosshole radar data,* Geophysics **72**, J53 (2007).

[13] J. Miksat, T. M. Müller, and F. Wenzel, *Simulating three-dimensional seismograms in 2.5-dimensional structures by combining two-dimensional finite difference modelling and ray tracing,* Geophysical Journal International **174**, 309 (2008).

[14] A. Yarovoy, R. de Jongh, and L. Ligthart, *Ultra-wideband sensor for electromagnetic field measurements in time domain,* Electronics Letters **36**, 1115 (2000).

[15] E. Slob, R. Maarsen, and R. Ghose, *Unified processing scheme for shared earth model inversion of GPR and seismic data,* in *EAGE 67th Conference & Exhibition - Madrid, Spain, 13 - 16 June* (2005).

[16] M. Frijlink and K. Wapenaar, *Reciprocity theorems for one-way wave fields in curvilinear coordinate systems,* SIAM Journal on Imaging Sciences **3**, 390 (2010).

[17] K. Wapenaar and J. van der Neut, *A representation for Green's function retrieval by multidimensional deconvolution,* Journal of the Acoustical Society of America **128** (2010).

[18] S. Minato, T. Matsuoka, and T. Tsuji, *Singular-value decomposition analysis of source illumination in seismic interferometry by multidimensional deconvolution,* Geophysics **78**, Q25 (2013).

[19] R. Feld and E. C. Slob, *GPR without a source by use of interferometry by multi-dimensional deconvolution,* (Society of Exploration Geophysicists, SEG-2014-1254, 2014) pp. 844–849.

[20] E. C. Slob and C. P. A. Wapenaar, *Electromagnetic Green's functions retrieval by cross-correlation and cross-convolution in media with losses,* Geophysical Research Letters **34** (2007).

[21] J. van der Kruk, C. P. A. Wapenaar, J. T. Fokkema, and P. M. van den Berg, *Three-dimensional imaging of multicomponent ground-penetrating radar data,* Geophysics **68**, 1241 (2003).

[22] A. Giannopoulos, *Modelling ground penetrating radar by GprMax,* Construction and Building Materials **19**, 755 (2005).

[23] R. Feld and E. C. Slob, *Sampling aspects of interferometry,* in *Proc. 15th Intl. Conference on Ground Penetrating Radar (GPR2014)* (IEEE, ISBN 978-1-4799-6789-6, 2014) pp. 592–597.

4

Line-array GPR monitoring without transmitting anything

Huygens' principle says that each pont on a wavefront behaves as a point source, and likewise with seismic interferometry we reduce the wave-front to a virtual point source at locations where physical receivers have measured a response. A line-array of receivers measures ambient noise and simultaneously its reflections and multiple reflections in the subsurface. Interferometric methods split what goes into the ground from what comes out of the ground, so that the signature of the subsurface remains after deconvolution or cross-correlation. The method does not use any information about the actual source's location. The source can be mobile phone radiation, already available in the air, as long as this background radiation can be represented by uncorrelated noise sources. Interferometry by deconvolution (IbD) removes the information from the original sources located at one side of the receivers and replaces them with virtual sources at the location of the original receivers. Interferometry by cross-correlation aims at removing the information of the original sources located all around two receivers and replace them by a virtual source at the location of one of the two receivers. A finite difference time-domain solver can create 3D line-array data of receiving antennas on the surface of a 2D subsurface model. The data is modeled as if it was generated by ambient noise sources that are all located in the air above the receiver line. By applying the IbD and CC techniques, the 2D GPR signal can be retrieved as if there would be a transmitting antenna at a receiving antenna's position. Numerical results show that both IbD and CC work well, even under strong spatial undersampling due to a shortage of receiving antennas or due to a large distance between subsequent receiving antennas

in the line-array. For this, it does not matter whether the air is crowded of noise or not, as long as the measurement records are long enough. The inverse problem of IbD is preferably solved with a singular values decomposition solution, rather than a least-squares solution, although this does not make much difference under strong spatial undersampling.

Parts of this chapter have been submitted to IEEE Transactions on Geoscience and Remote Sensing [1].

4.1. Introduction

The field of seismic interferometry is getting more and more known, and it gets advantageously applied to an increasingly wider field. Interferometric methods create virtual sources at physical receiver locations. In this way the effect of changing surface conditions can be minimized, if the receivers are positioned outside the influence of these surface conditions. Interferometry can be based on cross-correlation (CC) or deconvolution (IbD) techniques [2]. These techniques do not use any information about the actual source positions. Actual sources can be controlled, i.e. a transmitting antenna for GPR purposes, or uncontrolled. The latter type is called a passive source. In general passive sources are all sources that emit 'background' signals, for instance mobile phone radiation. The field that applies interferometric techniques to passive source data is known as passive interferometry. Passive GPR has already been validated numerically in 2D [3–5].

When one considers a line-array of receiving antennas, measuring the response of a transmitting antenna moving along a line, a 3D to 2D transformation is required. Such a transformation requires the physical source positions [6], as discussed in Chapter 3, while the interferometric methods itself do not use any physical source position information.

Here, we consider a plane of random noise sources and a line-array of receiving antennas. The plane of noise sources represents mobile communication radiation that is already present in the air. We show that in such a configuration no 3D to 2D transformation is required, so that no information about the physical source position is needed to be known for this analysis. Then, we continue by investigating the case of transient noise sources, to see what would happen in a sparser case. For practical reasons, we finish by investigating aliasing effects to obtain information on how much aliasing is tolerable in terms of accurate virtual source data retrieval.

4.2. Passive interferometry by deconvolution

The downgoing and upgoing wavefields, respectively $\hat{P}^+$ and $\hat{P}^-$, are connected by the reflection response $\hat{R}$ [7]:

$$\hat{P}^-(\boldsymbol{x}_r, \boldsymbol{x}_s, \omega) = \int_{\boldsymbol{x}\in\partial\mathbb{D}} \hat{R}(\boldsymbol{x}_r, \boldsymbol{x}, \omega)\, \hat{P}^+(\boldsymbol{x}, \boldsymbol{x}_s, \omega)\, d^2\boldsymbol{x}, \tag{4.1}$$

with angular frequency ω, source position $\boldsymbol{x}_s$, receiver position $\boldsymbol{x}_r$ and integration variable $\boldsymbol{x}$, which integrates over an infinite boundary $\partial\mathbb{D}$. The hat denotes a quantity in the frequency domain. This is the 3D version of (3.9). Eq. (4.1) shows that the reflection response $\hat{R}(\boldsymbol{x}_r, \boldsymbol{x}, \omega)$ is independent of the actual source position $\boldsymbol{x}_s$. The superposition principle lets us sum over all N_s actual source signals for a certain receiver position $\boldsymbol{x}_r$. For our situation of simultaneously acting random uncorrelated noise sources we define

$$\begin{cases} \hat{P}^-(\boldsymbol{x}_r, \omega) = \sum_{i=1}^{N_s} \hat{P}^-(\boldsymbol{x}_r, \boldsymbol{x}_{s,i}, \omega) \\ \hat{P}^+(\boldsymbol{x}', \omega) = \sum_{i=1}^{N_s} \hat{P}^+(\boldsymbol{x}', \boldsymbol{x}_{s,i}, \omega) \end{cases}, \tag{4.2}$$

x' are points like x_r, and i represents the actual source at position $x_{s,i}$. When the world is sufficiently homogeneous along one dimension, the 3D wave propagation for a line of sources summed along that dimension corresponds to the propagation initiated by a line source [8]. Hence, for a medium with a homogeneous dimension, (4.2) includes a kind of 3D to 2D transformation.

Using the similarities with the 2D case (3.9), here in 3D the reflection response (4.1) 'becomes'

$$\hat{\mathbf{R}} = \hat{\mathbf{P}}^{-}\left(\hat{\mathbf{P}}^{+}\right)^{\dagger}\left[\hat{\mathbf{P}}^{+}\left(\hat{\mathbf{P}}^{+}\right)^{\dagger}\right]^{-1} \tag{4.3}$$

in matrix notation. The † symbolizes the conjugated transpose of the matrix. Eq. (4.3) is known as *interferometry by deconvolution* (IbD). In view of (4.2) source-position information x_s is implicitly contained in $\hat{\mathbf{P}}^{+}$ and $\hat{\mathbf{P}}^{-}$ separately and through cross-correlation this information is removed in $\hat{\mathbf{P}}^{-}\left(\hat{\mathbf{P}}^{+}\right)^{\dagger}$ and $\hat{\mathbf{P}}^{+}\left(\hat{\mathbf{P}}^{+}\right)^{\dagger}$, because we assume that the noise sources are mutually uncorrelated. We use the Moore-Penrose pseudoinverse [9] to estimate the inverse term of (4.3) by a singular values decomposition solution (SVD). Singular values get organized in decreasing sequence in matrix $\hat{\mathbf{\Delta}}$. Values smaller than a certain value are replaced by zeros after inversion. When we write

$$\hat{\mathbf{P}}^{+}\left(\hat{\mathbf{P}}^{+}\right)^{\dagger} = \hat{\mathbf{U}}\hat{\mathbf{\Delta}}\hat{\mathbf{V}}^{\dagger} \text{ with } \hat{\mathbf{\Delta}} = \begin{pmatrix} \hat{\mathbf{\Delta}}_r & \hat{\mathbf{0}} \\ \hat{\mathbf{0}} & \hat{\mathbf{0}} \end{pmatrix}, \tag{4.4}$$

$\hat{\mathbf{\Delta}}_r$ the submatrix containing nonzero singular values and r the rank of $\hat{\mathbf{P}}^{+}\left(\hat{\mathbf{P}}^{+}\right)^{\dagger}$, then we can estimate [10]

$$\left[\hat{\mathbf{P}}^{+}\left(\hat{\mathbf{P}}^{+}\right)^{\dagger}\right]^{-1} \approx \hat{\mathbf{V}}\begin{pmatrix} \hat{\mathbf{\Delta}}_r^{-1} & \hat{\mathbf{0}} \\ \hat{\mathbf{0}} & \hat{\mathbf{0}} \end{pmatrix}\hat{\mathbf{U}}^{\dagger}, \tag{4.5}$$

in order to retrieve the reflection response by IbD. Alternatively we can use a least-squares solution [7] of (4.3)

$$\hat{\mathbf{R}} = \hat{\mathbf{P}}^{-}\left(\hat{\mathbf{P}}^{+}\right)^{\dagger}\left[\hat{\mathbf{P}}^{+}\left(\hat{\mathbf{P}}^{+}\right)^{\dagger} + \hat{\epsilon}\right]^{-1}, \tag{4.6}$$

with $\hat{\epsilon}$ a matrix with positive real numbers for stabilization on its diagonal. During the analysis of the data we will come back to this approach.

If we ignore matrix inversion in (4.3) we obtain the *interferometry by cross-correlation* (CC) result [11]

$$\hat{\mathbf{R}}_{CC} \approx \hat{\mathbf{P}}^{-}\left(\hat{\mathbf{P}}^{+}\right)^{\dagger}|S|^{-2}, \tag{4.7}$$

with $|S|^2$ the power spectrum of the source signature. In practice the amplitude of the CC retrieved wavelet will be normalized.

We assume that the fields are recorded on a line in which the world is homogeneous. Then the relation between the up- and downgoing wavefields and the measured electric and magnetic fields is one of spatial convolution. This spatial

convolution can be exploited in wavenumber domain as a product [6, 12] (Chapter 3, equations (3.7) and (3.8), here flux normalised):

$$\begin{cases} \tilde{P}^{+} = \sqrt{\frac{\Gamma}{\zeta}}\tilde{E}_x + \sqrt{\frac{\zeta}{\Gamma}}\tilde{H}_y \\ \tilde{P}^{-} = \sqrt{\frac{\Gamma}{\zeta}}\tilde{E}_x - \sqrt{\frac{\zeta}{\Gamma}}\tilde{H}_y \end{cases}, \tag{4.8}$$

with the tilde symbolizing the wavenumber-frequency domain, $\zeta = j\omega\mu$, $\Gamma = \sqrt{k_y^2 + (j\omega\varepsilon + \sigma)\,\zeta}$ and j the imaginary unit, μ the magnetic permeability, ε the permittivity, σ the conductivity and k_y is the horizontal wavenumber. The electric field strength can be measured with a GPR antenna, and the magnetic field with a loop antenna [13].

4.3. Simulation model

In a 10 x 10 x 3 m^3 container of sand a 1.85 m long metal pipe with a diameter of 9 cm is located at 0.5 m depth [14]. The sand is considered homogeneous with frequency independent properties and it has a relative electric permittivity of 3.1 [14]. These parameters are implemented using the 3D Finite Difference Time-Domain (FDTD) code GprMax [15]. GprMax considers media with frequency independent and isotropic properties.

We place 72 unshielded receivers in a line 2 cm below the surface, with 4 cm distance between each two receivers. Those receivers record the horizontal electric field-component perpendicular to the receiver-line, and the horizontal magnetic field-component parallel to the receiver-line. The record takes 52.9 microseconds. Reflection or absorption by the receivers are not taken into account, because these are just filtering effects that do not change the interferometric principles that we want to validate. In practice the receivers will be mounted to a plastic stand to fix their positions with respect to each other, but this is likewise not considered in the simulation model, because it will not change the interferometric principles.

In Europe the frequencies of our interest for mobile phone communication are 2 x 65 MHz bandwidth in the 800 and 900 MHz bands [16]. Such a narrow bandwidth causes ringing in the time-domain. Without affecting the interferometric methods we consider a wider bandwidth, so that ringing does not occur. To mimic background mobile phone communication signals, 3774 random noise sources are regularly distributed in a horizontal plane of 3 x 2 m^2, forming one big noise-plane 0.1 m above the surface, such that the pipe lays below the middle, orientated along the longer dimension of the plane. We assume that this plane of sources represents most of the incoming directions of noise of a real situation. Fig. 4.1 shows the configuration schematically. Also the desired virtual source position is marked.

The noise sources are band-limited by a Ricker wavelet with a center frequency of 900 MHz. Their phase is random, and hence we refer to them as random noise sources. To consider sparsely ambient noise in the air, we also simulate transient

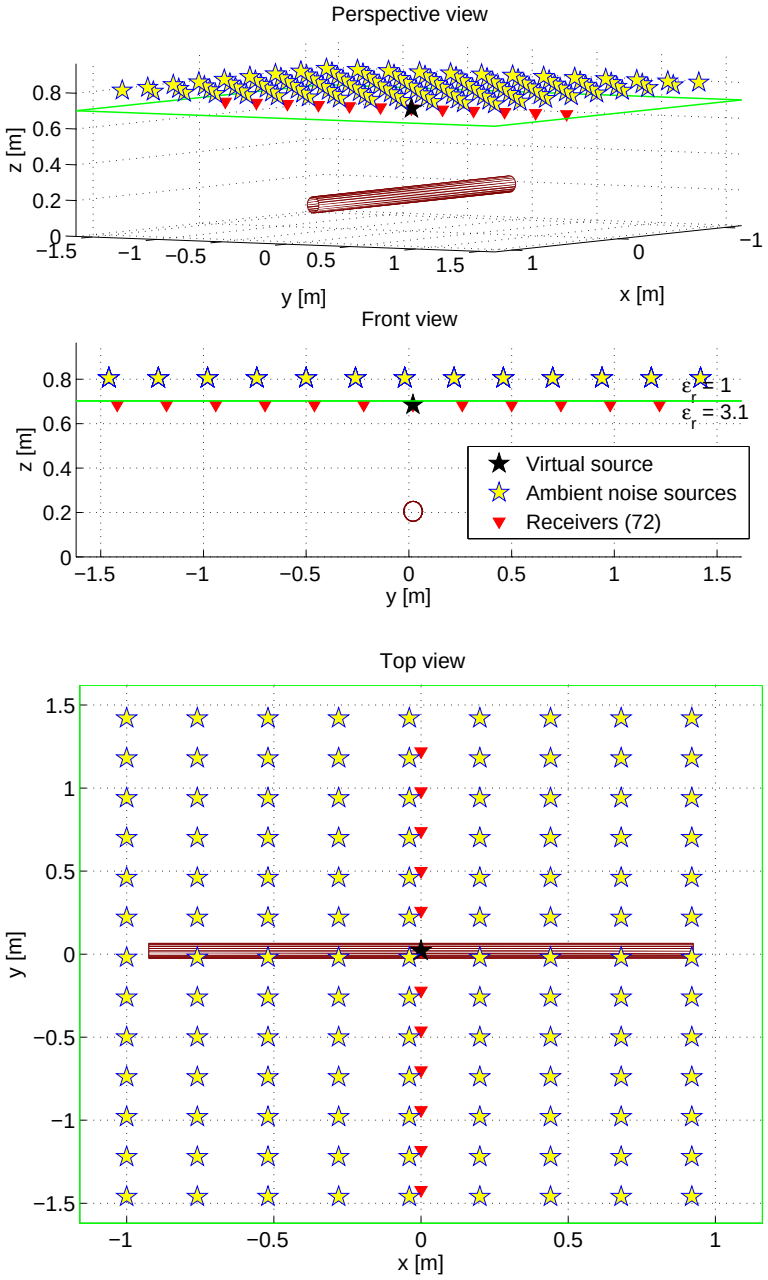

Figure 4.1: Schematic display of the linesetup. There is a pipe in a homogeneous sand ground. Noise sources are simulated in a 3 x 2 m^2 plane. Receivers are placed along a line, perpendicular to the metal pipe. The Earth's surface is drawn as a green line/rectangle. The virtual source will be created on the position of the middle receiver. To cope with the high amount of transmitting and receiving antennas, only some antenna positions are indicated in this scheme.

noise sources. With transient noise sources, exactly one pulse is emitted at a random time by each source, so that the activity in the air is minimal.

4.4. Numerical results

4.4.1. Random noise sources

Fig. 4.2 shows some traces of the horizontal electric and magnetic components, due to simultaneously acting random noise sources, recorded by the middle receiver. Now, note that the configuration is chosen such that the world does not change much along the pipe, see Fig. 4.1. Therefore we expect that the record, which is the summation of the signals emitted by all the noise sources with and without reflections, includes a kind of 3D to 2D transformation, so that we can continue with 2D interferometric formulations. In other words, the physical situation already transforms the 3D data to nearly 2D during the measurement, and therefore provide us nearly 2D horizontal electric and magnetic field components. We use these components to determine the downgoing wavefields and the upgoing wavefields with (4.8). Fig. 4.3 shows these wavefields with respect to one time-trace for different receiver positions. The downgoing field is clearly noise. The pipe acts as a secondary source, due to its cylindrical shape, as can be recognized in the upgoing field. The decomposition step appeared very sensitive for little displacements, which would result in an incomplete separation of the upgoing and downgoing fields. It is therefore recommended to mount the antennas to a hardened plastic stand to prevent any vertical displacements and to ensure the determined distances in the array.

Then, with (4.3) we retrieve by IbD the signal response with respect to a virtual source at the position of the middle receiver. Singular values smaller than 30% of the largest singular value are made zero after inversion (4.5). This choice influences the amplitude of the retrieved signal and of the clutter level. Lowering the clutter level increases the risk of influencing the retrieved signal too much. Here our choice comes from trial and error when we optimize the result to be as close to the ideal result as possible. Also the least-squares solution (4.6) is optimized by trial and error. It provides the result with a relatively large error before the arrival, but less clutter after the arrival. Still, the singular values decomposition solution is notably more appealing and therefore shown in Fig. 4.4. The combination of both solutions would improve the result, but that is not done here. We compare the IbD result with the ideal output and the CC output in Fig. 4.4. The data is analyzed using Matlab [17].

For our situation Snell's law's critical angle is 34.6°. This means that the range on the surface from which rays reach the object and add to the IbD result is less than 0.78 m long. Note that due to the pipe's shape, its reflection is recorded by every receiver and therefore their data is useful at any position. The IbD output contains lots of clutter, what might be reduced by optimizing the length of the assumed time-window for a source.

The distance between the line of receivers and the farthest sources along the pipe (along the shorter dimension of the plane) might be insufficient, although the

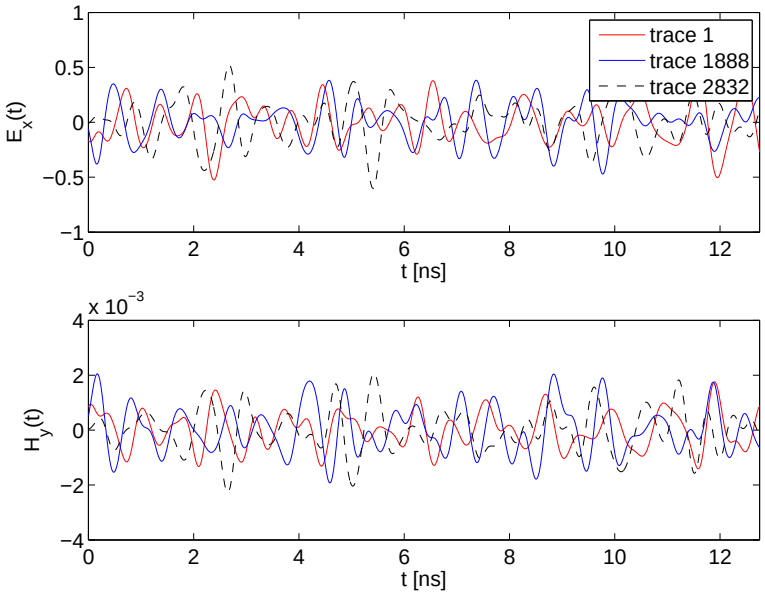

Figure 4.2: Some time-traces of the electric and magnetic fields originating from random noise sources received by the middle receiver.

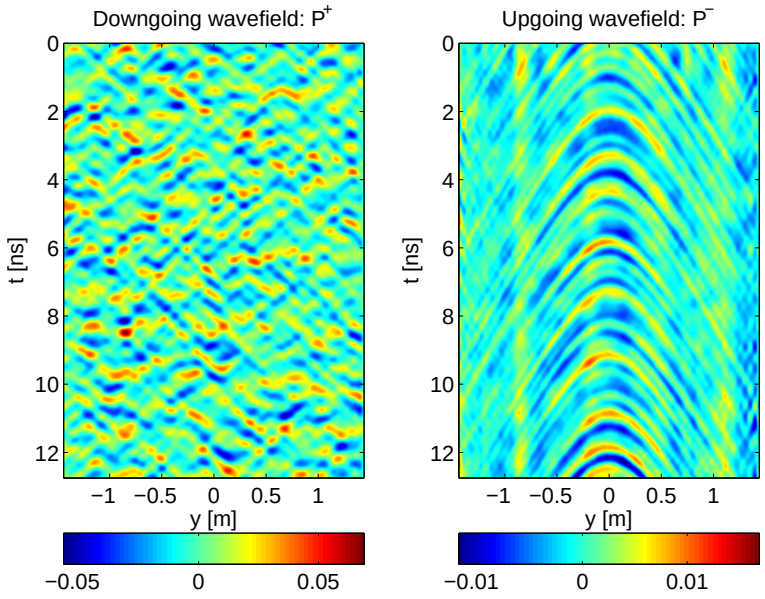

Figure 4.3: The down- and upgoing wavefields originating from random noise sources with respect to one of the time-traces for different receiver positions.

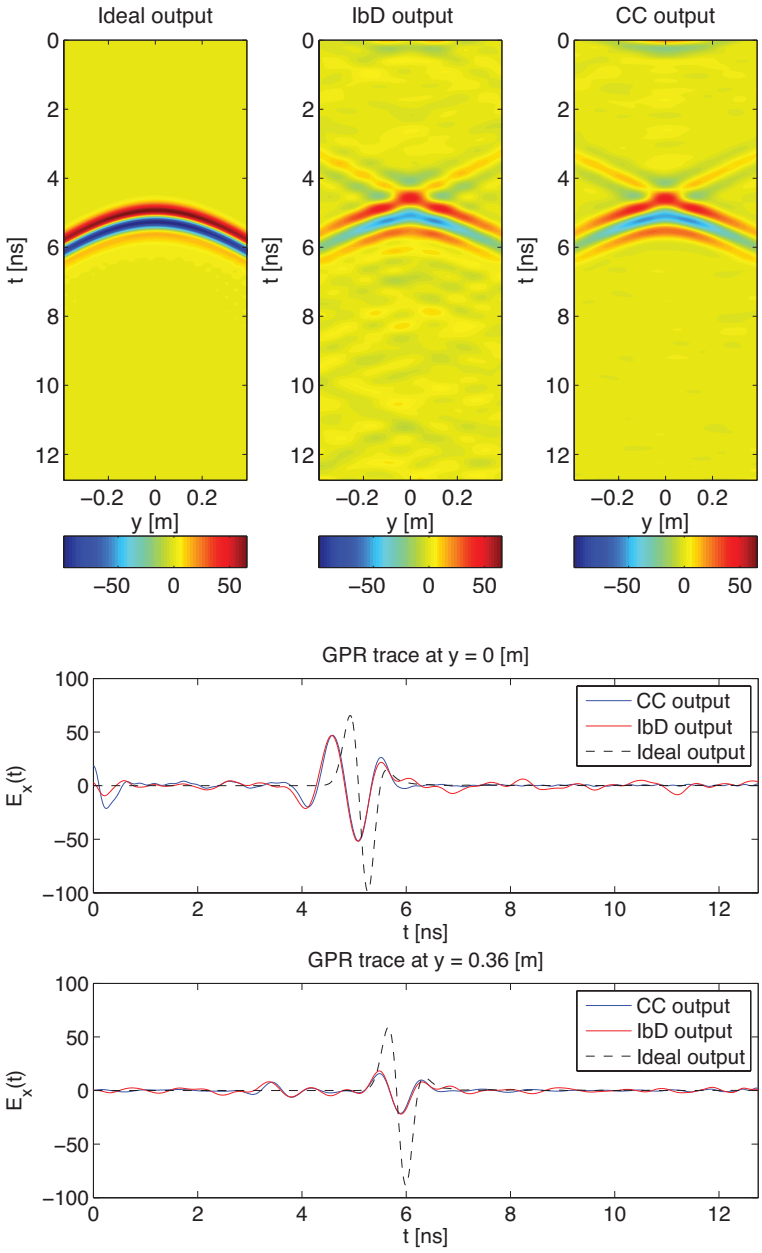

Figure 4.4: Random noise is received. Shown here is the comparison of the response after a virtual source created by interferometry by deconvolution (IbD) and interferometry by cross-correlation (CC) with the case of a real source on this position (ideal case).

corresponding cut-off error of a sudden end of sources does not coincidence with the main signal after summation. Moreover, the ideal output is found by assuming an infinite pipe and infinite line-sources, modeled in 2D, and is therefore not an optimal comparison, but we do not have a better alternative. It is the best comparison, because we want to be able to treat the data as 2D data. With the actual configuration this might not be optimal to achieve this, but that is not something changeable. These can cause the differences between the IbD and CC outputs with the reference output. Note that the slight time-shift for both IbD and CC is also found for controlled sources (Chapter 3) [6], and that the result looks like what is found in 2D [5].

The CC output's amplitude has been normalized to the IbD output's amplitude, because the CC method only provides phase information, whereas the IbD method provides amplitude information itself. The time-reversed event before the arrival in the CC output is a characteristic of this method [18].

For practical purposes, the same procedure has been repeated for three other line-configurations with less receivers and more distance between the receivers. See Fig. 4.5 for their IbD outputs. For the configurations with 70 ($0.8\lambda_{min}$ = 4 cm), 24 ($2.5\lambda_{min}$ = 12 cm) and 18 ($3.4\lambda_{min}$ = 16 cm) receivers, with the corresponding in-between distances between receivers mentioned between brackets expressed in the smallest local wavelength, singular values smaller than 30% of the of the largest singular value are made zero after inversion. For the configuration with 36 ($1.7\lambda_{min}$ = 8 cm) receivers the threshold was set at 33%. Obviously, increasing the sampling distance leads to reducing the output quality. It is up to the user to decide whether the result is still acceptable, or that a denser line-setup with more receivers is desired. For each configuration both the singular values decomposition (SVD) and least-squares (lst-sqr) solutions have been optimized and compared. It turns out that for the configurations with 70, 36 and 24 receivers the SVD solution provides a IbD output that looks more like the ideal output. However, the SVD solution seems to worsen quicker than the least-square solution, and for the configuration of only 18 receivers both provide a reasonable IbD output (and this latter is therefore shown in Fig. 4.5). Fig. 4.6 compares the CC outputs of the different configurations. The absolute maximum value of the CC output of each configuration has been normalized to the absolute maximum value of the IbD output of the same configuration. Obviously, also here the output worsens with worser sampling.

4.4.2. Transient noise sources

Fig. 4.7 shows some traces for the horizontal electric and magnetic components, due to transient noise sources. Each transient source emits once at a random time. The receiver does not measure the direction, but only the phase and amplitude. It does not discriminate between different signals. Therefore, traces can be without signal or with one or more signals if multiple signals transmit around the same time. This is for instance respectively the case for traces 1, 1888 and 2832 in Fig. 4.7. The procedure is exactly the same as for random noise sources. The data is decomposed in downgoing wavefields and upgoing wavefields with (4.8). Fig. 4.8 shows these

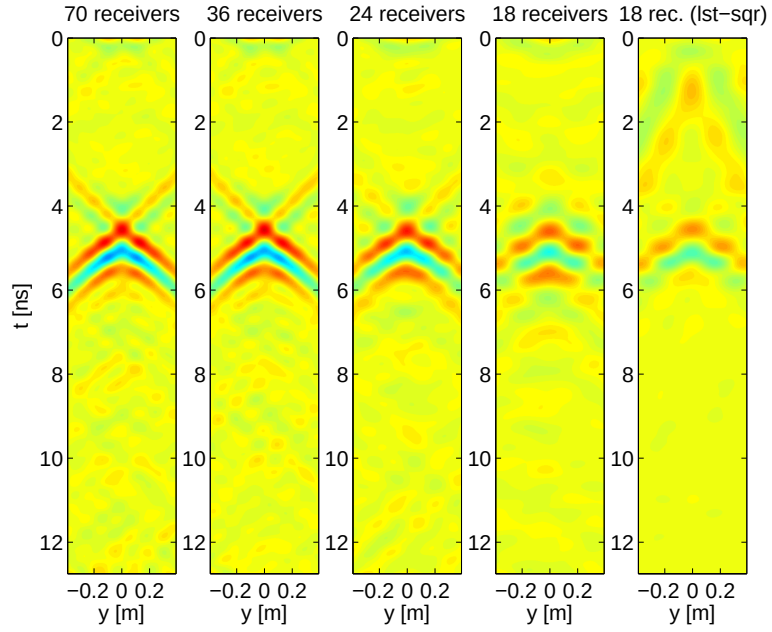

(a)

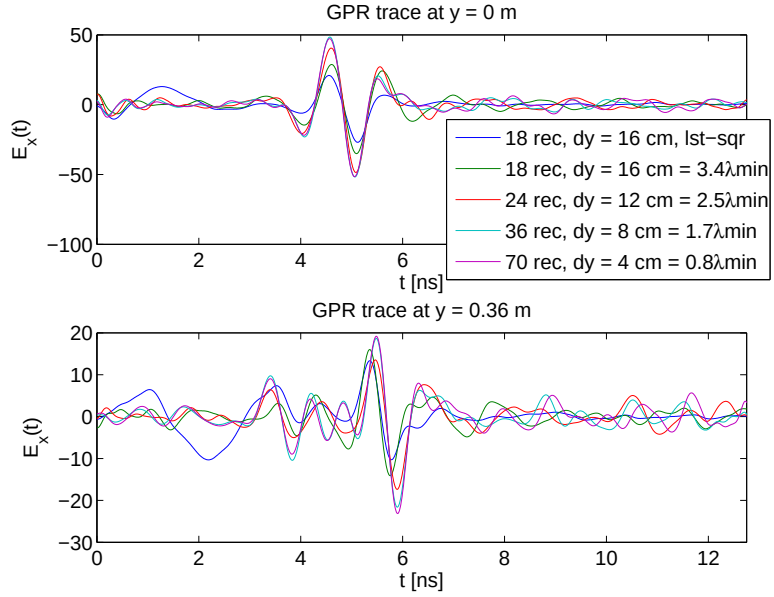

(b)

Figure 4.5: Comparison of the response after a virtual source created by IbD using random noise source-data measured by different configurations existing of different receiver amounts (with different inner distances expressed in the smallest wavelength): 70 ($0.8\lambda_{min}$ = 4 cm), 36 ($1.7\lambda_{min}$ = 8 cm), 24 ($2.5\lambda_{min}$ = 12 cm) and 18 ($3.4\lambda_{min}$ = 16 cm). The 18 receivers configuration is also considered using the least-squares solution (lst-sqr) for IbD. Fig. 4.5a: All graphs are shown w.r.t. the same colorbar.

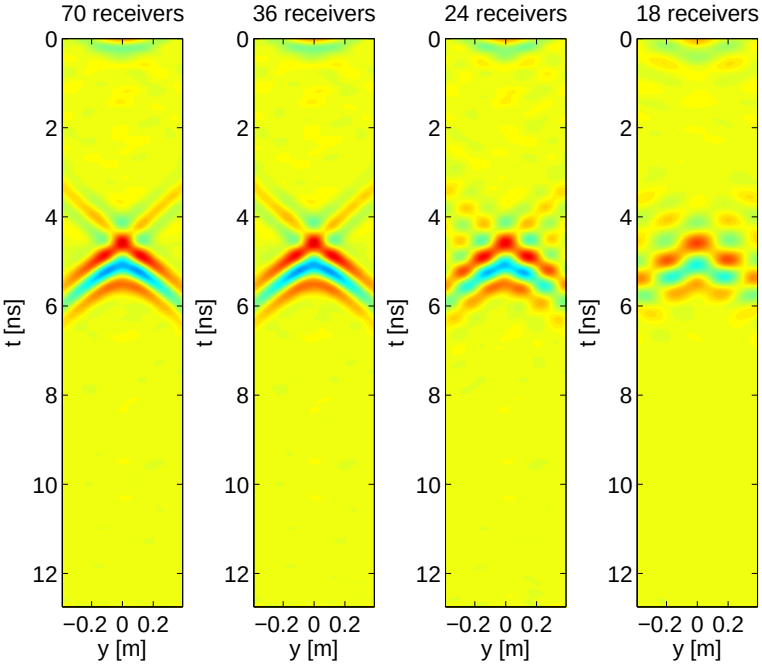

Figure 4.6: Comparison of the response after a virtual source created by CC using random noise source-data measured by different configurations existing of different receiver amounts (with different inner distances expressed in the smallest wavelength): 70 ($0.8\lambda_{min}$ = 4 cm), 36 ($1.7\lambda_{min}$ = 8 cm), 24 ($2.5\lambda_{min}$ = 12 cm) and 18 ($3.4\lambda_{min}$ = 16 cm). All graphs are shown w.r.t. the same colorbar.

wavefields with respect to one time-trace for different receiver positions. In this particular time-trace the receiver at 0.9 m first records a signal. The pipe acts as a secondary source again. Note that some other effects are visible, which might point at some leakage during decomposition. The data used for this article is corrected spatially and temporally for the staggered grid of the FDTD-solver. Still, the FDTD-solver only approximates the time by discretizing the world, while decomposition requires a high temporal resolution. This makes leakage not unlikely to occur. With (4.3) we retrieve by interferometry by IbD the signal response with respect to a virtual source at the position of the middle receiver. Singular values smaller than 24% of the largest singular value are made zero after inversion (4.5). We compare the IbD result by transient noise sources with the ideal and CC outputs in Fig. 4.9. The results look remarkably similar as the results found for the case of random noise sources, which means that it does not matter whether the air is crowded with noise or not, as long as you measure long enough. Note that the transient source result is not that symmetric as the random noise result, when considering the clutter. This is expected to improve with longer records.

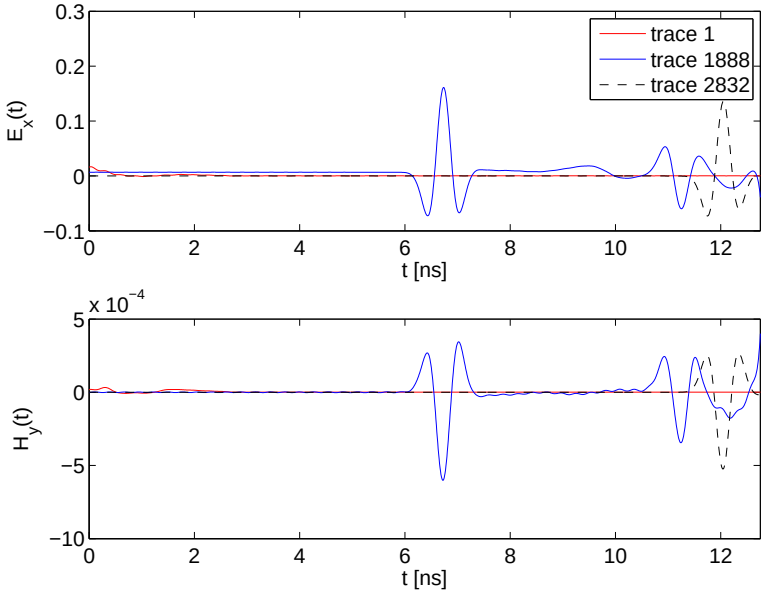

Figure 4.7: Some time-traces of the electric and magnetic fields originating from transient noise sources received by the middle receiver.

Also for the case of transient noise sources the three other configurations of 36 ($1.7\lambda_{min}$ = 8 cm), 24 ($2.5\lambda_{min}$ = 12 cm) and 18 ($3.4\lambda_{min}$ = 16 cm) have been considered in Fig. 4.10, with the corresponding in-between distances between receivers mentioned between brackets expressed in the smallest local wavelength. For the configurations with 70, 36 and 18 receivers, singular values smaller than 24% of the of the largest singular value are made zero after inversion. For the

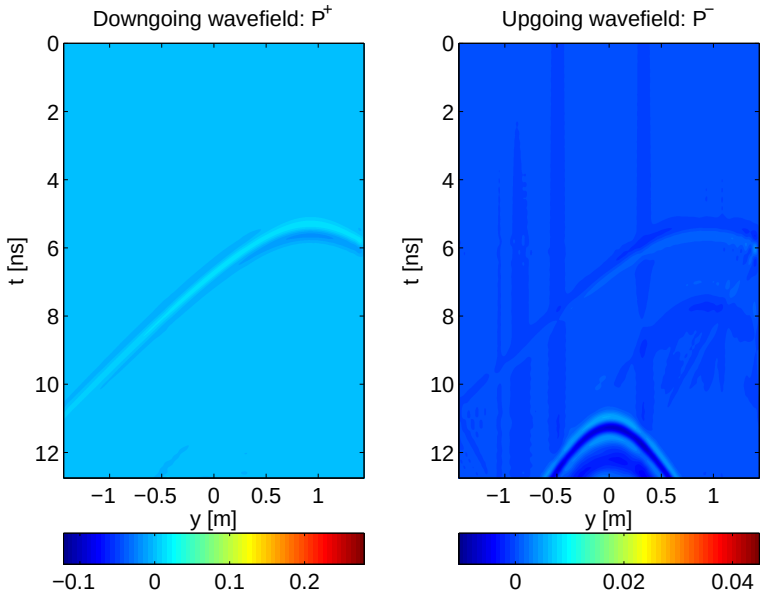

Figure 4.8: The down- and upgoing wavefields originating from transient noise sources with respect to one of the time-traces for different receiver positions.

configuration with 24 receivers this number is taken 30%. Obviously, a worse sampling results in a worse output. As said before for the case of random noise sources, it is up to the user to decide whether the result is still acceptable, or that a denser line-setup with more receivers is desired. For each setup both the singular values decomposition (SVD) and least-squares (lst-sqr) solutions have been optimized and compared. For the configurations with 70, 36 and 24 receivers the SVD solution provides a better IbD output. Also here is noted that the SVD solution seems to worsen quicker than the least-square solution, and for the configuration of only 18 receivers both provide a well IbD output (this latter is therefore shown in Fig. 4.10. The CC outputs from the different setups are shown in Fig. 4.11. Also here the absolute maximum value of the CC output of each configuration has been normalized to the absolute maximum value of the IbD output of the same configuration. Obviously, also here the output worsens with worser undersampling.

4.5. Discussion

4.5.1. Benefits for GPR

Applying seismic interferometry to GPR has many advantages. One advantage is the GPR measurement without transmitting any signal. This applies to cases where transmitting is not possible or unwanted. Then the measurement is also not restricted by the FCC rules.

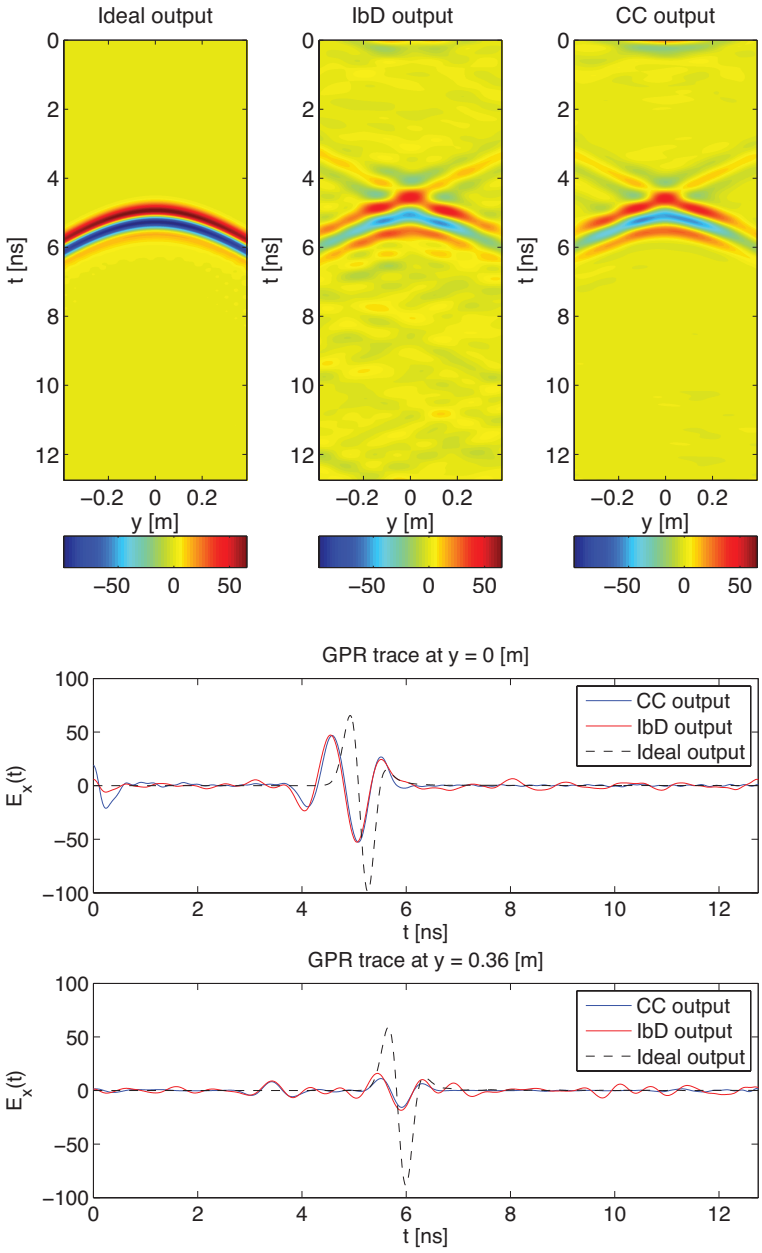

Figure 4.9: Transient noise is received. Shown here is the comparison of the response after a virtual source created by interferometry by deconvolution (IbD) and interferometry by cross-correlation (CC) with the case of a real source on this position (ideal case).

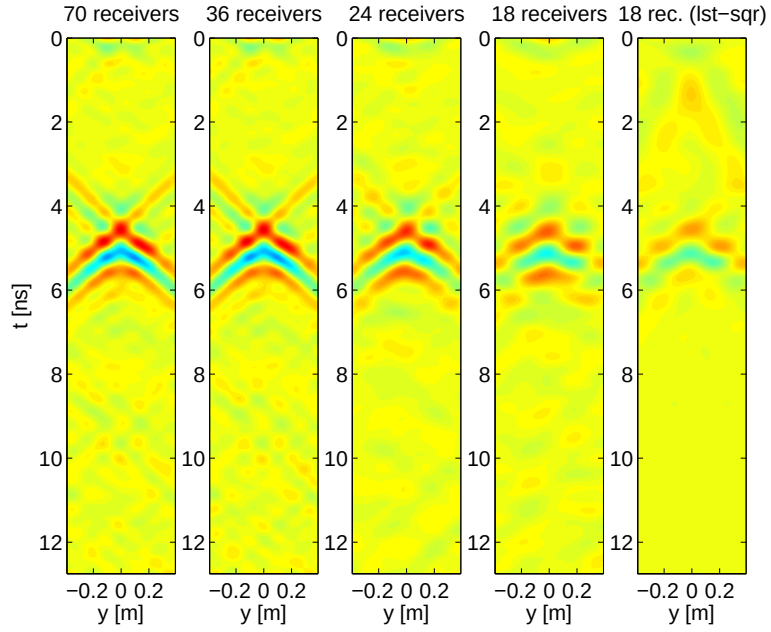

(a)

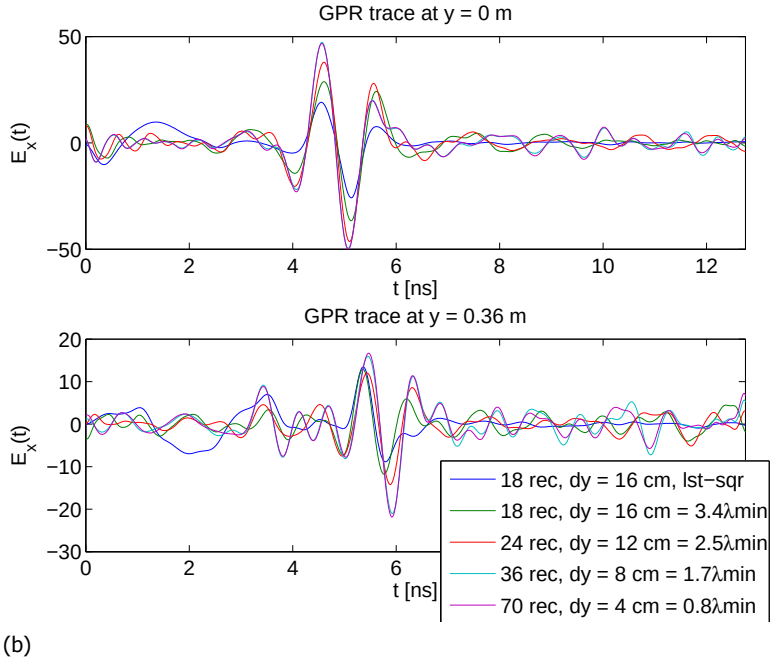

(b)

Figure 4.10: Comparison of the response after a virtual source created by IbD using transient noise source-data measured by different configurations existing of different receiver amounts (with different inner distances expressed in the smallest wavelength): 70 ($0.8\lambda_{min}$ = 4 cm), 36 ($1.7\lambda_{min}$ = 8 cm), 24 ($2.5\lambda_{min}$ = 12 cm) and 18 ($3.4\lambda_{min}$ = 16 cm). The 18 receivers configuration is also considered using the least-squares solution (lst-sqr) for IbD. Fig. 4.10a: All graphs are shown w.r.t. the same colorbar.

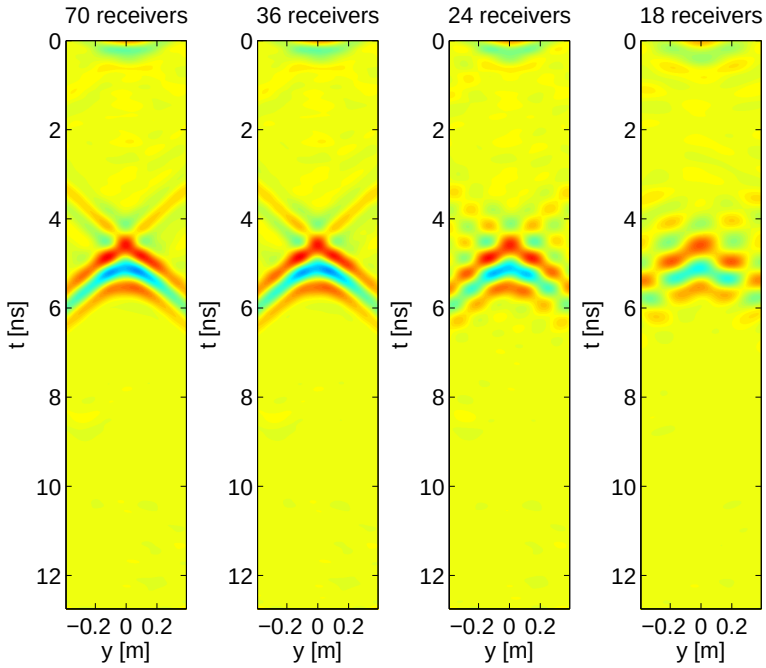

Figure 4.11: Comparison of the response after a virtual source created by CC using transient noise source-data measured by different configurations existing of different receiver amounts (with different inner distances expressed in the smallest wavelength): 70 ($0.8\lambda_{min}$ = 4 cm), 36 ($1.7\lambda_{min}$ = 8 cm), 24 ($2.5\lambda_{min}$ = 12 cm) and 18 ($3.4\lambda_{min}$ = 16 cm). All graphs are shown w.r.t. the same colorbar.

Another advantage is that the interferometry by IbD method homogenizes the world above the receiver array. When the receiver array is placed below the surface, the effects of changing surface conditions are minimized during monitoring measurements. Likewise, the receiver array can be placed below the water table, so that the IbD method removes the water table out of the data. Then, in order to measure signals that are strong enough to pass the water table, one could retrieve the Green's function from a controlled source experiment, or one could generate noise by a controlled source, like is done in noise radar. As a side note, noise radar transmits a controlled random phased signal and correlates a time-delayed version of the transmitted signal with the received signal [19, 20], while in this article we consider uncontrolled, external sources.

Traditional passive radar also uses external sources, and then determines location and velocity of objects by cross-correlating the direct and reflected signals. However, in GPR the illumination aperture is strongly limited by Snell's law, and the ground is dissipative. The IbD method can deal with dissipation, which is therefore an essential benefit when applied to GPR data. The method retrieves both amplitude and phase information, whereas the CC method retrieves phase information only.

4.5.2. Challenges

In practice there are some challenges. Here, we address what are the challenges at this moment, and what are not challenges, and why.

In practice we deal with a narrow 2 x 65 MHz bandwidth in the 800 and 900 MHz bands [16], causing ringing in time-domain. This ringing will not influence the interferometric methods, but it does not make the retrieved result easy to interpret, and it can even mask structures. Therefore, we should not limit us to mobile phone signals only, but consider a wider frequency band of ambient noise sources. In fact, the whole frequency spectrum is filled with sources, such that the use of frequencies is actively managed [21].

One might think that the ambient noise should be sufficiently active. However, comparing random and transient noise results in this article, which are the extremes of ambient noise activity in the air, shows that it does not matter whether the air is crowded with noise or not, as long as you measure long enough.

One aspect of importance is the amplitude of the ambient noise. Chapter 2 [22] mentions the typical electromagnetic field strength of 0.5 - 3 V/m on the street [23]. Then, they use a heterogeneous pavement model in a 2D world to estimate the field strength of approximately 0.0471 V/m of the signal that reflected at the depth of their interest. After this they conclude that the reflected electromagnetic field strength is measurable. The amplitude of the ambient noise is therefore not a challenge.

An easily overlooked technological challenge is the real-time measurement. We are dealing with uncontrolled sources. This means that we cannot use subsampling, because the source signal is constantly changing, and so we require real-time gigasampling to measure the arrival times. If one alternatively prefers to use the frequency spectrum, then all frequencies need to be measured at the exact same

time. Because otherwise the different frequencies originate from different sources, and then no coherent signal is recorded. Interferometry requires a coherent signal. Real-time measurements are nowadays still a technological challenge in GPR. Real-time measurements with frequencies of about 600-900 MHz are possible, depending on the parameter settings. The lowest frequency band for mobile phone communication in Europe lays around 900 MHz. It is a matter of time until such a measurement is within technological reach. Higher frequencies can be measured real-time, but than the amount of bits is very low. In the field of noise radar the transmitted signal is known, and in that case low-bit analog-to-digital convertors (ADCs) can be used advantageously [20]. However, in the case of seismic interferometry with uncontrolled source the transmitted signal is unknown. Only the sum of direct and (multiple) reflected waves are known. Hence, the technique of low-bit ADCs does not apply here.

This section shows that the advantages of applying seismic interferometry to GPR can be large, that it is definitely worth researching it. Also, for the case of mobile phone signals as sources, it is just a matter of time before the method can be applied.

4.5.3. Applications

A receiver array is placed just below the surface. Interferometry is applied to retrieve the reflection response with respect to a virtual source at one of the receiver positions, like if the world above the receiver array is homogeneous, while the actual sources can be background electromagnetic waves, for example those used by mobile communication. Advantages can be found in cases where the use of a source is impossible, forbidden, or cumbersome, while using a receiver-array is possible. The method is specifically advantageous for monitoring applications, because here it is desirable to leave receivers in the same set up for time-lapse measurements over longer timescales [4].

4.6. Conclusion

Our numerical work shows that, if receiving antennas are in close contact to the subsurface, and the world is sufficiently homogeneous along one dimension, a 2D GPR measurement can be performed with receiving antennas in a line-array, without transmitting a source signal. The actual source might be, for instance, mobile phone radiation, already available in the 3D world. This can be achieved by use of interferometry by deconvolution (IbD) or interferometry by cross-correlation. Good results can also be retrieved with spatially undersampled data, and hence the amount of receivers can be reduced, or the in-between distance of each two receivers enlarged. Although undersampling affects the output negatively, it is up to the user's requirements how many receivers suffice. The IbD result looks best when the singular values decomposition (SVD) solution is applied, but for highly undersampled data both SVD and least-squares solutions provide comparable outcomes. A combination of these both solutions might reduce the clutter a bit more, but this has not been applied because the results look already satisfactory.

Another important conclusion is that it does not matter whether the air is crowded with noise or not, as long as you measure long enough. The follow-up research will experimentally apply GPR without a source.

References

[1] R. Feld and E. C. Slob, *Line-array GPR monitoring without transmitting anything,* IEEE Transactions on Geoscience and Remote Sensing (2016).

[2] K. Wapenaar, E. Slob, R. Snieder, and A. Curtis, *Tutorial on seismic interferometry: Part 2 - Underlying theory and new advances,* Geophysics **75**, 75A211 (2010).

[3] E. Slob, D. Draganov, and K. Wapenaar, *Let the FCC rules work for you: Turning commercial noise into useful data,* (GPR2006 conference, Columbus Ohio, USA, 2006).

[4] J. Li, Z. Zeng, E. C. Slob, X. Chen, and F. Liu, *Simulation of GPR passive interferometry using cross-correlation for LNAPL model monitoring application,* Geophysical Journal International **199**, 1919 (2014).

[5] R. Feld and E. Slob, *GPR without a source by use of interferometry by multidimensional deconvolution,* in *SEG-2014-1254: Society of Exploration Geophysicists conference* (Denver Colorado, USA, 2014) pp. 844–849.

[6] R. Feld and E. C. Slob, *Validation of interferometry applied to GPR by simulation of possible experimental line-configurations,* IEEE Journal of Selected Topics in Applied Earth Observations and Remote Sensing (submitted).

[7] E. C. Slob, *Interferometry by deconvolution of multicomponent multioffset GPR data,* IEEE Transactions on Geoscience and Remote Sensing **3** (2009).

[8] J. Miksat, T. M. Müller, and F. Wenzel, *Simulating three-dimensional seismograms in 2.5-dimensional structures by combining two-dimensional finite difference modelling and ray tracing,* Geophysical Journal International **174**, 309 (2008).

[9] S. Minato, T. Matsuoka, and T. Tsuji, *Singular-value decomposition analysis of source illumination in seismic interferometry by multidimensional deconvolution,* Geophysics **78**, Q25 (2013).

[10] W. Menke, *Geophysical data analysis: discrete inverse theory*, International Geophysics, vol. 45, revised edition, pp. 119-125 (Academic press, ISBN-13: 978-0-12-490921-2, 1989).

[11] K. Wapenaar, E. Slob, and R. Snieder, *Seismic and electromagnetic controlled-source interferometry in dissipative media,* Geophysical Prospecting **56**, 419 (2008).

[12] R. Feld and E. C. Slob, *Sampling aspects of interferometry,* in *Proc. 15th Intl. Conference on Ground Penetrating Radar (GPR2014)* (IEEE, ISBN 978-1-4799-6789-6, 2014) pp. 592–597.

[13] A. Yarovoy, R. de Jongh, and L. Ligthart, *Ultra-wideband sensor for electromagnetic field measurements in time domain,* Electronics Letters **36**, 1115 (2000).

[14] J. van der Kruk, C. P. A. Wapenaar, J. T. Fokkema, and P. M. van den Berg, *Three-dimensional imaging of multicomponent ground-penetrating radar data,* Geophysics **68**, 1241 (2003).

[15] A. Giannopoulos, *Modelling ground penetrating radar by GprMax,* Construction and Building Materials **19**, 755 (2005).

[16] M. J. M. Verhagen, *Strategische nota mobiele communicatie en beschikbaar stellen 800 MHz band voor mobiele breedband*, Tech. Rep. (Ministry of economic affairs in The Netherlands, http://www.rijksoverheid.nl/bestanden/documenten-en-publicaties/kamerstukken/2010/12/10/strategische-nota-mobiele-communicatie-en-beschikbaar-stellen-800-mhz-band-voor-mobiel-breedband/10184648.pdf, 2010).

[17] Matlab, *R2013a (8.1.0.604), 64-bit (maci64)* (The MathWorks Inc., 2013).

[18] E. Slob and K. Wapenaar, *Electromagnetic Green's function retrieval by cross-correlation and cross-convolution in media with losses,* Geophysical Research Letters **34** (2007).

[19] R. M. Narayanan, Y. Xu, P. D. Hoffmeyer, and J. O. Curtis, *Design, performance, and applications of a coherent ultra-wideband random noise radar,* Optical Engineering **37**, 1855 (1998).

[20] S. R. J. Axelsson, *Noise radar for range/doppler processing and digital beamforming using low-bit ADC,* IEEE Transactions on Geoscience and Remote Sensing **41** (2003).

[21] *Staat van de Ether 2013*, Tech. Rep. (Radiocommunications Agency Netherlands (Agentschap Telecom), Ministry of Economic Affairs, The Netherlands, 2014).

[22] R. Feld, E. C. Slob, and J. W. Thorbecke, *Non-destructive pavement damage inspection by mono-static GPR without transmitting anything,* (submitted).

[23] Antennebureau, *The information agency of the Dutch government concerning antennas*, Tech. Rep. (http://www.antennebureau.nl/onderwerpen/algemeen/veldsterktemetingen, website kept up-to-date).

5

Discussion

Either you love me or you hate me...

Anonymous

Chapters 2 up to 4 describe research performed on electromagnetic interferometry in the frequency range used for ground-penetrating radar. The practical possibilities are explored. Chapter 2 investigates mono-static ground-penetrating radar (GPR) for pavement damage inspection without transmitting anything. Mono-static refers to the use of exactly one antenna, and therefore interferometry by cross-correlation reduces to auto-correlation, which is just the squared amplitude of the recorded data. In the case of multiple antennas cross-correlation is useful, as has been shown in chapters 3 and 4. A possible extension could be to consider sources on both sides of a bridgedeck for inspection. Interferometry with two sided illumination has been researched by Li et al. [1], but not for bridgedeck inspection. The bridge should be rather plastic fiber based so that illumination adds from both sides.

In chapters 2 up to 4 we considered Ricker shaped sources with a centre frequency of 900 MHz, which is around the mobile phone frequency bandwidth. In this chapter we briefly explore another application: Tunnel detection by GPR at broadcast radio frequencies without transmitting anything.

Different techniques are available for localization of tunnels, mines, or buried objects. Lo Monte et al. [2] propose radio frequency tomography above other methods for tunnel detection. GPR is not considered as reliable or practical in tunnel detection for several reasons. One argument is that the frequency spectrum can be limited by broadcasting stations and other external sources. Active source seismic interferometry is applied for tunnel detection by Kaslilar et al. [3]. A possible application of electromagnetic interferometry in the GPR frequency range could be to use broadcasting signals that are already available in the air to look into the

ground with frequencies that traditional GPR is not allowed to use. This would be much quicker and cheaper than seismic measurements. Every car already has an antenna to receive radio signals. Turn such an antenna horizontal on a border patrol car and one might inspect for tunnels during a usual border inspection. However, the question is whether sufficient signal penetrates the subsurface to measure a reflection. Broadcasting antennas are orientated such that their signals radiate as far as possible above the ground. One might discuss whether it is ethical or not to improve a tunnel detection tool for border security.

Another possible application of electromagnetic interferometry in the GPR frequency range are passive measurements used for GPR research on Mars [4]. On Earth the atmosphere stops a part of cosmic background radiation, but Mars does not has an atmosphere like on Earth. Cosmic background radiation might be an ideal source for passive interferometry. Traditional GPR measurements emit radiation and this costs energy. Instead, with passive interferometry it is only necessary to receive, so that the Mars rover requires less energy during mapping of the shallow subsurface.

References

[1] J. Li, Z. Zeng, E. C. Slob, X. Chen, and F. Liu, *Simulation of GPR passive interferometry using cross-correlation for LNAPL model monitoring application,* Geophysical Journal International **199**, 1919 (2014).

[2] L. Lo Monte, D. Erricolo, F. Soldovieri, and M. C. Wicks, *Radio frequency tomography for tunnel detection,* IEEE Transactions on Geoscience and Remote Sensing **48**, 1128 (2010).

[3] A. Kaslilar, U. Harmankaya, K. Wapenaar, and D. Draganov, *Estimating the location of a tunnel using correlation and inversion of Rayleigh wave scattering,* Geophysical Research Letters **40**, 6084 (2013).

[4] S.-E. Hamran, T. Berger, S. Brovoll, L. Damsgård, Ø. Helleren, M. J. Øyan, H. E. Amundsen, L. Carter, R. Ghent, J. Kohler, M. Mellon, D. Paige, D. Plettemeier, and J. Eide, *RIMFAX: a GPR for the Mars 2020 Rover Mission,* in *8th International Workshop on Advanced Ground Penetrating Radar (IWAGPR), 7-10 July, Florence, Italy* (2015).

6

Conclusion

Retrieving virtual source responses at physical receiver locations by interferometry by deconvolution (IbD) or cross-correlation (CC) can be beneficial for monitoring applications, or applications where the use of a source is impossible, forbidden, or cumbersome, while using receivers is possible. When the actual source positions might change during subsequent measurements, interferometry has the benefit of retrieving the response of virtual sources at fixed and known locations and orientations. With interferometry less measurements are required, since it can retrieve responses with respect to different virtual source positions, saving operational costs Placed below the groundwater table, IbD removes temporal variations in the partially saturated overburden. The accuracy of interferometric results is not as good as when a real source is used at the receiver's location, but all information is still interpretable.

6.1. Non-destructive pavement damage **inspection by mono-static GPR** without transmitting anything

For modeling studies of interferometry by auto-correlation (AC), applied to damaged pavement, the medium parameters can be varied along one or two dimensions. The heterogeneous model along one dimension is recommended, given that such a model is easier to implement and run through, while the second varying dimension does not improve the result tremendously. The source distribution, measurement time, and temporal distribution of the noise sources only influence the interferometric results to a limited extent. The actual sources might be uncontrolled mobile phone signals, already available in the air. The result is sufficient for all interpretations possible with the conventional use of GPR. Regarding the noise and pavement models we used, the concept of non-destructive pavement damage inspection by auto-correlation of mono-static GPR noise data seems realistic and

feasible. The next step is to validate this concept with actual noise recordings in the field.

6.2. **Line-array GPR monitoring**: virtual source data reconstruction from possible experimental configurations

In this part of the research receivers in a line-configuration measure 3D data by a controlled source. After transforming this data to 2D, 2D interferometry by deconvolution and by cross-correlation can be carried out. The 3D to 2D transformation has a worse effect on the accuracy of the result, than undersampling. However, the result is still interpretable, and the interferometric methods provide advantages, such as reducing the operation costs. The cross-correlation method is not negatively affected by having sources only on one side. The next step is to retrieve virtual reflection responses from real data to investigate the scenario closer to its field application.

6.3. **Line-array GPR monitoring** without transmitting anything

This part of the research considers receivers in a line-configuration measuring 3D data by uncontrolled sources. If the world is sufficiently homogeneous along one dimension, no 3D-to-2D is required prior to the use of 2D interferometry. 2D GPR measurements can be performed in a 3D world, without transmitting anything. The actual sources might again be uncontrolled mobile phone signals, which are already available in the air. Even with spatially undersampled data good results can be retrieved. Although undersampling does affect the output negatively, it is up to the user's requirements how many receivers suffice. The singular values decomposition solution (SVD) is preferred for IbD, except for higly undersampled data, then both SVD and least-square solutions provide comparable outcomes. It does not matter whether the air is crowded with noise or not, as long as you measure long enough. The follow-up research is to apply GPR without a source in the field, since numerical results look promising for geometries that look homogeneous, such as pipeline inspection.

This thesis provided practical ideas for electromagnetic interferometry applied to GPR, and proposed configurations for experiments and the belonging expectations by numerical modeling. The possibility to subtract useful signal out of electromagnetic noise data seems feasible.

Epilogue

Blame it on the night,
don't blame it on me

Calvin Harris song featuring John Newman, 2014

I don't know any other way to show
It's not getting any better
I think we both know that there's something wrong
When we keep holding on to the best days

Armin van Buuren song, 2015

In The Netherlands gaining a PhD degree is not seen as status, and it will not necessarily help in getting a job, in contrary to others parts in the world. Often, it is seen as overqualification, making it hard to get hired. Recruiters interpret it as if you suddenly stop your academic career, while at the university the PhD is seen as just a degree. It requires more research to find a suitable job. The developed skills can be used in many disciplines, but the PhD, in order to make a chance, needs to actively sell his or her qualities well-advertised when applying for a job. When I talk about developed skills during the PhD, think about delivering a certain quality, project-management, documenting, reporting, and presenting in a clear way, and software/programming skills.

I finish this thesis mentioning three notes I wished I took the following earlier into the acuteness of my consciousness:

- I do the things, because I want it, or to meet expectations of others?
- I'm only responsible for myself, every aspect of my life, and not for other's.
- Enjoy each moment fully since tomorrow can be different. Don't wait.

Acknowledgements

The sun is shining
and so are you

Axwell and Ingrosso song, 2015

First I express my feelings of gratitude to Alessandra Daggiano. In 2014 we both visited the United States of America for the first time for a holiday. Due to unfortunate circumstances my research required work during this 'vacation', so that I daily worked between 4 and 7 in the morning, and 8 and 12 during the night, so that during the other hours I was available for our meant-to-be-relaxing holiday. This is just one of the examples of me being absent both physically and mentally. Having earned the doctoral degree, I make sure such days are gone. I thank you Sandra for your remarkable patience and love. I am fluent in Italian language, and well-known with its culture, thanks to you and your family.

Special thanks go to Bart van Horssen and Richard Spek for the refreshing discussions about life and self-development. These discussions positively influenced my growth-curves in all areas of life, so that I particularly could focus more on the context of my PhD-research. I also thank other friends for similar discussions.

Effective progression requires relaxation. It was always a pleasant break with office mates Shohei Minato, Huajun Fan, Mohammad Chahardowli, and Rahul Thorat. Huajun and Mohammed taught me elementary Mandarin and Persian; and we traditionally chitchatted in seven different languages as office culture. I used to share the office with Huajun, and we covered the walls with Chinese vocabulary! For over a decade I got my weekly required relaxation from divers self-defense workouts by Dick van Wijngaarden. These trainings, including the well-known oliebollentraining, I'll miss the most when I move out of Delft.

I express my gratitude to Evert Slob, who has been my supervisor during the PhD-process. I appreciate how Evert, despite of his busy schedule, quickly responded on mails, and that I could always just pass by his office. He always came with well, and teachable suggestions. One particular example was when I was writing my first conference article. Evert didn't tell me what to do, but how I could teach myself to write a clear article. I noticed how I grew from a PhD-student to an independent researcher under your supervision. And, Evert, thank you of course for making this PhD project possible.

With Fabio Tosti I cooperated to make a short-term mission in Rome possible. He managed to gather all required instruments from the GPR industry and an external sponsor for the short-term mission. However, there was too much time necessary

to develop an experimental setup from fundamental research. Hence, I missed out on this great opportunity. I thank him for his effort.

AD, PAE, and AL, despite faith separating us by the long distances, you've had a lasting influence on my personal development. You helped me see the direction where I wanted to go, when I couldn't see it. Thank you! From my heart, I hope all the best for you!

I thank the committee members for their feedback on this thesis.

Last, but certainly not least, I hereby express my gratitude to all colleagues internationally in the field of ground-penetrating radar, and at Delft University of Technology.

Ralph Feld
Delft, July 2016

Academic Curriculum Vitæ

Ralph Feld

6 Nov 1986	Born in Poortugaal, The Netherlands

Education

Apr 2011 – Apr 2016	**PhD** in Applied Geophysics, Delft University of Technology – Thesis subject: *Validation of Electromagnetic-Interferometry Applied to Ground-Penetrating Radar* – Self-taught software/programming skills; LaTeX, Linux, Matlab
Sep 2009 – Jan 2010	Minor Industrial Design, Faculty Industrial Design, TU Delft
Sep 2007 – Jul 2009	**MSc** in Applied Physics, TU Delft – Thesis subject: *Development of Instrumentation for Assessment of Radioactivity in Excreted Urine*
Sep 2004 – Jul 2007	**BSc** in Applied Physics, TU Delft – Thesis subject: *Analyse Intensity of Zero-Mode Waveguides to Study Single Molecule Activity of Telomerase* – Average mark BSc: 8.1 – Propedeuse cum laude – Minor Extension Science, Faculty Applied Physics, TU Delft – Minor Astronomy (first year), Leiden Observatory, Leiden University

Awards

July 2014	*Best Paper Poster Presentation*, International Conference on Ground Penetrating Radar, Brussels, Belgium

Languages

Fluent:	Dutch, English, Italian
Intermediate:	German
Basic:	French, Polish

Presentations and peer-reviewed conference papers

5. San Francisco, California, USA, American Geophysical Union (AGU) Fall Meeting, Dec 2015, *Mono-static GPR without transmitting anything: Interferometry by auto-correlation applied to mobile phone signals for non-destructive pavement damage inspection*, **R. Feld**, E. C. Slob, and J. W. Thorbecke

4. Florence, Italy, International Workshop on Advanced Ground Penetrating Radar (IWAGPR), Jul 2015, DOI: 10.1109/IWAGPR.2015.7292612, *Line-array GPR monitoring without transmitting anything*, **R. Feld** & E. C. Slob

3. London, UK, European Cooperation in Science and Technology (COST) meeting, Mar 2015, *Validation of interferometry applied to GPR by simulation of possible experimental line-configurations*, **R. Feld** & E. C. Slob

2. Denver, Colorado, USA, Society of Exploration Geophysics (SEG) Annual Meeting, Oct 2014, document ID: SEG-2014-1254, *GPR without a source by use of interferometry by multi-dimensional deconvolution*, **R. Feld** & E. C. Slob

1. Brussels, Belgium, International Conference on Ground Penetrating Radar (GPR2014), Jul 2014, ISBN: 978-1-4799-6789-6, *Sampling aspects of interferometry*, **R. Feld** & E. C. Slob

List of Publications

3. **R. Feld**, E.C. Slob, and J.W. Thorbecke, *Non-destructive pavement damage inspection by mono-static GPR without transmitting anything*, Geophysical Journal International (submitted 2016).

2. **R. Feld** and E.C. Slob, *Line-array GPR monitoring without transmitting anything*, IEEE Transactions on Geoscience and Remote Sensing (submitted 2016).

1. **R. Feld** and E.C. Slob, *Interferometric virtual source GPR data reconstruction by simulation of possible experimental line-configurations*, IEEE Journal of Selected Topics in Applied Earth Observations and Remote Sensing (submitted 2015).